

Abdul Rehman

## **Identification of Flux Maps at Constant Speed for Synchronous Motors**

**School of Electrical Engineering**

Thesis submitted for examination for the degree of Master of Science in Technology.

22.05.2017

**Thesis supervisor:**

Prof. Marko Hinkkanen

**Thesis advisor:**

Hafiz Asad Ali Awan, M.Sc. (Tech.)

Author: Abdul Rehman

Title: Identification of Flux Maps at Constant Speed for Synchronous Motors

Date: 22.05.2017

Language: English

Number of pages:6+45

Department of Electrical Engineering

Professorship: Electrical Drives

Code: S-3016

Supervisor: Prof. Marko Hinkkanen

Advisor: Hafiz Asad Ali Awan, M.Sc. (Tech.)

The accurate identification of flux linkages and inductances play a vital role in developing high-performance control methods for synchronous motors (SMs). In this thesis, the identification of flux maps of SMs at constant speed is done. The aim of this thesis is to achieve look-up tables of flux linkages as a function of machine currents. Simulation are performed on a 6.7-kW synchronous reluctance motor (SyRM). The current controlled SyRM, operating at constant speed, is fed with current sequences and the corresponding voltages are calculated. By using these calculated voltages, the motor flux linkages are identified and stored in the form of look-up tables. The iron losses and stator resistance variation are compensated during the identification process. These linkage look-up tables can be used as a benchmark for testing different saturation models of synchronous motors. From these look-up tables, the information about motor inductances can be obtained which can be used to fully exploit the motor torque and speed range by determining various control strategies such as the maximum torque per ampere (MTPA) and maximum torque per volt (MTPV).

Keywords: Flux maps, identification, saturation, look-up table, synchronous reluctance motors (SyRMs), permanent magnet assisted synchronous reluctance motors (PM-SyRMs)

# Preface

At the outset, I would like to offer my gratitude to Almighty ALLAH, the most Merciful, the most Gracious, the most High for giving me the strength, motivation to complete this thesis.

I would like to thank my thesis supervisor Prof. Marko Hinkkanen for providing me with this wonderful opportunity to work on this interesting topic. It has been an utmost pleasure working under his supervision.

I would also like to acknowledge my thesis instructor Asad bhia, for his constant guidance throughout the thesis. I would also like to thank Rano, Ahmad, Ammad and Rishi for keeping my company during the awesome lunch breaks.

Lastly, I would like to thank my Amma and Abba for their endless support and prayers for me. It would never have been possible without your love, prayers and support. I dedicate this thesis in memory of my late brother Salman, gone but never forgotten.

Otaniemi, 22.05.2017

Abdul Rehman

# Contents

<b>Abstract</b>	<b>ii</b>
<b>Preface</b>	<b>iii</b>
<b>Symbols and abbreviations</b>	<b>v</b>
<b>1 Introduction</b>	<b>1</b>
1.1 Background . . . . .	1
1.2 Goal and Outline of the Thesis . . . . .	3
<b>2 Modelling of Synchronous Motors</b>	<b>4</b>
2.1 Types of Synchronous Motors . . . . .	4
2.2 Space Vectors . . . . .	6
2.3 Modelling of Synchronous Motors . . . . .	7
2.4 Saturation . . . . .	9
2.5 Torque Generation in Synchronous Motors . . . . .	11
<b>3 Identification Techniques</b>	<b>13</b>
3.1 Standstill Identification Methods . . . . .	13
3.2 Self-Commissioning Techniques . . . . .	14
3.2.1 Self-Commissioning at Standstill Conditions . . . . .	14
3.2.2 Self-Commissioning at Free Shaft . . . . .	15
3.3 Constant Speed Identification Methods . . . . .	16
3.4 Reference Current Generation . . . . .	23
3.5 Flux Map Calculation . . . . .	27
3.6 Current Controller . . . . .	29
<b>4 Results</b>	<b>31</b>
4.1 Saturation Model . . . . .	33
4.2 Data Saving Algorithm . . . . .	35
4.3 Simulation Results . . . . .	36
4.3.1 Case 1 . . . . .	36
4.3.2 Case 2 . . . . .	36
4.3.3 Case 3 . . . . .	37
<b>5 Conclusions</b>	<b>40</b>
<b>References</b>	<b>42</b>

# Symbols and abbreviations

## Symbols

Boldface letters represent the matrices and the vectors. Reference values are marked by the subscript ref.

$dq$	Rotating or synchronous coordinates
$\mathbf{i}_s$	Stator current real space vector in synchronous coordinates
$i_s$	Magnitude of stator current real space vector
$i_d$	d-axis component of the stator current
$i_q$	q-axis component of the stator current
$\mathbf{i}_s^s$	Stator current real space vector in space vector coordinates
$L_s$	Stator inductance
$\mathbf{J}$	Orthogonal rotation matrix
$\mathbf{L}_s$	Inductance matrix
$L_d$	Direct-axis inductance
$L_q$	Quadrature-axis inductance
$p$	number of pole pair
$R_s$	Stator resistance
$u_d$	d-axis component of the stator voltage
$u_q$	q-axis component of the stator voltage
$\mathbf{u}_s$	Stator voltage real space vector in synchronous coordinates
$u_s$	Magnitude of stator voltage real space vector
$\boldsymbol{\psi}_s$	Stator flux real space vector in synchronous coordinates
$\psi_d$	d-axis component of the stator flux
$\psi_q$	q-axis component of the stator flux
$\boldsymbol{\psi}_{pm}$	Permanent-magnet flux vector
$\psi_{pm}$	Permanent-magnet flux
$T_e$	Electromagnetic torque
$\vartheta_m$	Electrical angle
$\omega_m$	Electrical angular speed
$\alpha\beta$	Space vector coordinates
$f_s$	Switching frequency
$i_{d,ref}$	Reference d-axis component of stator current
$i_{q,ref}$	Reference q-axis component of stator current

$i_{d,\max}$	Maximum d-axis component of stator current
$i_{q,\max}$	Maximum q-axis component of stator current
$\Delta i_d$	Step change in reference d-axis component of stator current
$\Delta i_q$	Step change in reference q-axis component of stator current

## Operators

## Abbreviations

SM	Synchronous motor
PM	Permanent magnet
PMSM	Permanent magnet synchronous motor
SyRM	Synchronous reluctance motor
PM-SyRM	Permanent magnet assisted synchronous reluctance motor
SPM	Surface-mounted permanent magnet motor
PI	Proportional integral
MTPA	Maximum torque per ampere
MTPV	Maximum torque per volt

# 1 Introduction

## 1.1 Background

The demand for energy has been on the rise for the last few decades. Electrical energy is a clean and efficient energy source that is favorable to environment as well as easy to transmit and control. Electric machines play a vital role both in the production and consumption of energy as they are used as motors and generators for conversions between electrical and mechanical energy [1]. A motor converts electrical energy to mechanical while a generator transforms mechanical energy to electrical. Induction motors (IMs) are used worldwide to convert electrical energy into useful mechanical work, while most of the world's electrical power is produced with the help of synchronous generators [1].

Gradually, synchronous motors (SMs) are becoming popular in comparison with IMs due to their low costs and high ruggedness [2]. The widely known types of SMs include permanent magnet synchronous motors (PMSMs), synchronous reluctance motors (SyRMs) and permanent magnet assisted synchronous reluctance motors (PM-SyRMs) [3–7]. Furthermore, PMSMs can be divided into surface-mounted permanent magnet motors (SPMs) and interior permanent magnet motors (IPMs). In SPMs, permanent magnets (PMs) are mounted on the surface of the rotor while in IPMs, the PMs are embedded in the slots cut inside of the rotor. High flux density and high coercivity are the desirable characteristics of PMs to be used in constructing these motors.

In SyRMs, the rotor consists of various paths for flux passing as well as multiple flux barriers are also present. One of these paths has a high permeability and other one a low permeability, commonly referred as the d- and q-axis respectively. There are no PMs present in the rotor of SyRMs, resulting in low inertia and low manufacturing costs. The ripples in torque and low power factor are the major drawbacks of SyRMs. In order to overcome these issues, PMs are placed in the rotor core of SyRMs resulting in PM-SyRMs.

Various rare-earth metals, like dysprosium (Dy) and neodymium (Nd) which fulfill

the criteria of high coercivity are used as magnetic materials for building PMSMs, but they are quite expensive [8]. The neodymium magnet (NdFeB) is amongst the most popular PMs till present, it is constructed by combining an alloy of neodymium with iron and boron. Since last few years, there has been a rapid increase in the price of NdFeB which demanded the need for the search of alternative PMs. Ferrite and AlNiCo magnets have emerged as suitable replacements for NdFeB [9]. Both of these magnets have lesser coercivity in comparison with NdFeB but they are quite cheap. More volumes of ferrite magnets can be used in PMSMs to get almost the same efficiency as NdFeB [10]. It can be said that a compromise between performance and cost is needed when it comes to the selection of PMs for PMSMs.

Due to various advantages such as low torque ripple, reduced losses, and low production costs in comparison with PMSMs, PM-SyRMs can be used in different high performance industrial applications such as the aerospace actuators, pumping, industrial and vehicle traction systems [10, 11]. On the other hand, one of the major downsides of PM-SyRMs along with SyRMs are the extreme self and cross saturation conditions which are required to produce the high torque density. In extreme saturation conditions, the motor inductances vary in terms of the motor currents or flux linkages, an efficient saturation magnetic model is required to overcome this problem.

An accurate magnetic model is a backbone for the control of an AC motor. The relationship between the currents and flux linkages define the magnetic model of any specific motor. The most commonly used frame for representing SMs is rotor synchronous (dq) frame [5, 11–13]. The precise identification of stator flux linkages and inductances play a vital role in developing high performance control methods for SMs. The evaluation of flux linkages is challenging, particularly for motors operating in deep saturation such as SyRMs and PM-SyRMs [5]. Along with the saturation effect caused by the self-axis current, significant cross-saturation effect is also present in these motors. Furthermore, the presence of space and switching harmonics also complicates the magnetic model identification process [11].

Until now, numerous magnetic model identification techniques for different kinds of SMs have been proposed in literature. For SyRMs and PM-SyRMs at standstill condition, current in one axis (e.g., in the q-axis) is maintained constant while a voltage pulse is supplied to the other axis (e.g., in the d-axis) and the flux linkages are then computed from the integration of the voltage induced in the stator [5, 14, 15]. The inaccurate estimate of stator resistance reduces the accuracy of the estimated flux linkages. On the other hand, constant currents are applied to PMSMs and SyRMs running at constant speed, to evaluate the flux linkages by measuring the output voltages [4, 11]. An efficient parameter identification process is the one, that takes into account the self and cross-saturation conditions, stator resistance estimate, inverter voltage drop, and iron losses of the motor.

## 1.2 Goal and Outline of the Thesis

The goal of this thesis is the identification of flux maps at constant speed for SMs. The main objective is to create look-up tables of flux linkages as a function of machine currents which could be used as a benchmark for testing different saturation models of SMs. A current controlled SyRM, operating at constant speed, is fed with current sequences and the corresponding voltages are calculated. By using these calculated voltages, the motor flux linkages are identified and stored in the form of look-up tables. The stator resistance variation and iron losses are compensated during the flux linkages calculations. Both, the self and cross-saturation conditions are taken into consideration while populating the look-up tables. From these look-up tables, useful knowledge about the motor inductances can be obtained which could be helpful in designing high performance control methods for SMs.

The thesis is divided into five sections. The structure of SMs, a brief review of space vectors and the modelling of SMs in the synchronous reference (dq) frame is explained in Section 2. The torque generation and the saturation characteristics of SMs are also discussed in Section 2. In Section 3, the existing experimental magnetic model identification methods of SMs are described. Both, the standstill and constant speed magnetic model identification techniques are reviewed in detail. Section 4 presents the results obtained through the simulations performed in MATLAB/Simulink environment. Finally, Section 5 gives an overview of the conclusions deduced from the results.

## 2 Modelling of Synchronous Motors

Depending upon the construction of the rotor, magnetically SMs can be mainly categorized into salient and non-salient pole motors. Salient pole motors can be further classified into two types, IPMs which have the PMs embedded in the rotor and SyRMs which have no PMs in their rotor. PM-SyRMs have PMs employed in the hollow flux barriers present in the rotor, combining the properties of SyRMs and IPMs. The presence of the PMs in the rotor increases the length of the effective air gap in the magnetic axis, generally referred as the d-axis. Usually, the PMs used in SMs have almost the same relative permeability as that of air,  $\mu_r = 1.05$ . The saliency of these motors is increased by PMs as they act as free space alongside the path used by the flux to pass. In this chapter, a review of space vectors, the structure of SyRMs and PM-SyRMs and the typical saturation characteristics of SMs have been briefly discussed. Furthermore, various modelling approaches of SMs have also been explained.

### 2.1 Types of Synchronous Motors

A conceptual diagram of a four pole SyRM is presented in Figure 2.1. SyRMs have a laminated constructed stator which consists of a 3-phase distributed winding. The lamination of SyRMs helps in reducing the core losses. Since the last few years, SyRMs with transverse laminated rotors have become more popular owing to their robust structure and low costs [2, 6]. In SyRMs, the stator currents create the rotating magnetic field with the motor running at synchronous speed. The rotor tries to align with the rotating magnetic field in order to find the path that offers the least amount of reluctance. When the rotor reaches close to the synchronous speed, it gets magnetically locked by the stator magnetic field in the minimum reluctance position. The torque produced by this phenomenon is known as the reluctance torque. The rotor of the SyRM consists of several flux barriers, these flux barriers are constructed for limiting the flux along the q-axis and for attaining a greater saliency ratio. SyRMs have a robust construction and require less maintenance.

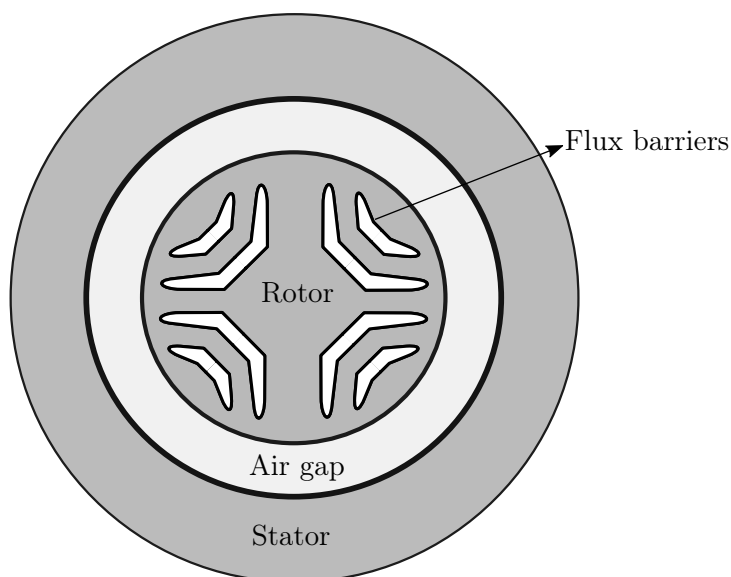


Figure 2.1: A four pole SyRM.

For increasing the power factor and reducing the torque ripple, PMs are placed inside the rotor flux barriers of SyRMs, resulting in the formation of PM-SyRMs. The overall torque produced in PM-SyRMs is the combination of the reluctance torque and the torque produced by the PMs. PM-SyRMs are often referred as IPMs, when the flux produced by PMs contributes more towards the overall flux produced in the motor. A conceptual diagram of a four pole PM-SyRM is shown in Figure 2.2.

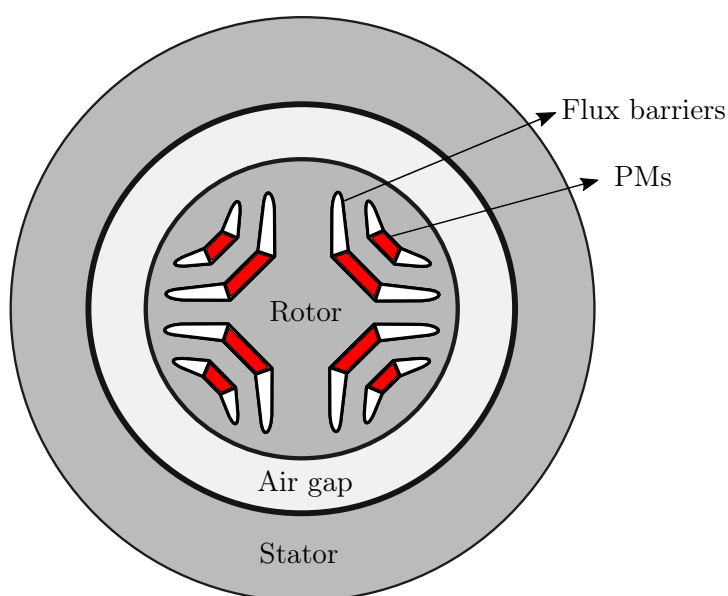


Figure 2.2: A four pole PM-SyRM.

## 2.2 Space Vectors

The three-phase currents can be described in terms of a space vector. The  $\alpha\beta$  coordinates are used for the representation of the space vector. The transformation of the three-phase current into the space vector components is given as

$$\mathbf{i}_s^s = \begin{bmatrix} \frac{2}{3} & \frac{-1}{3} & \frac{-1}{3} \\ 0 & \frac{1}{\sqrt{3}} & \frac{-1}{\sqrt{3}} \end{bmatrix} \begin{bmatrix} i_a \\ i_b \\ i_c \end{bmatrix} \quad (2.1)$$

where  $i_a, i_b, i_c$  represent the three-phase currents while  $\mathbf{i}_s^s$  is the stator current real space vector in space vector and it is given as

$$\mathbf{i}_s^s = \begin{bmatrix} i_\alpha \\ i_\beta \end{bmatrix} \quad (2.2)$$

Whereas, the conversion to three-phase currents from the space vector components is represented as

$$\begin{bmatrix} i_a \\ i_b \\ i_c \end{bmatrix} = \begin{bmatrix} 1 & 0 \\ \frac{-1}{2} & \frac{\sqrt{3}}{2} \\ \frac{-1}{2} & \frac{-\sqrt{3}}{2} \end{bmatrix} \mathbf{i}_s^s \quad (2.3)$$

The flux linkages and voltages can also be transformed into the  $\alpha\beta$  coordinates by using the same approach. In order to control the speed and torque of SMs, the three-phase currents are controlled with the help of three-phase voltages supplied to the motor. These three-phase currents and voltages are usually converted into space vector form and afterwards they are transformed into the rotor synchronous (dq) coordinate system. When the phase voltages and currents are converted into the dq coordinates they can be viewed as DC components in the steady state conditions.

With the rotor position angle  $\vartheta_m$  given as

$$\vartheta_m = \int_0^t \omega_m dt \quad (2.4)$$

the transformation from the  $\alpha\beta$  to dq coordinates is given as

$$\mathbf{i}_s = e^{-\mathbf{J}\vartheta_m} \mathbf{i}_s^s \quad (2.5)$$

where  $\mathbf{i}_s$ , the stator current real space vector in synchronous coordinates is given as

$$\mathbf{i}_s = \begin{bmatrix} i_d \\ i_q \end{bmatrix} \quad (2.6)$$

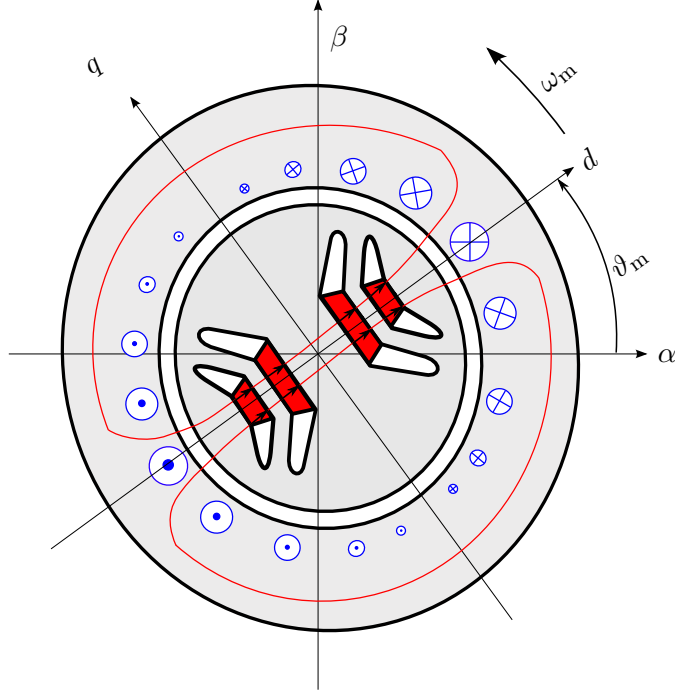


Figure 2.3: Conceptual diagram of a two pole three phase PM-SyRM.

while the orthogonal rotation matrix  $\mathbf{J}$  is given as

$$\mathbf{J} = \begin{bmatrix} 0 & -1 \\ 1 & 0 \end{bmatrix} \quad (2.7)$$

and the transformation matrix  $e^{-\mathbf{J}\vartheta_m}$  is given as

$$e^{-\mathbf{J}\vartheta_m} = \begin{bmatrix} \cos(\vartheta_m) & \sin(\vartheta_m) \\ -\sin(\vartheta_m) & \cos(\vartheta_m) \end{bmatrix} \quad (2.8)$$

### 2.3 Modelling of Synchronous Motors

The conceptual diagram of a two pole three-phase PM-SyRM, with PMs buried inside the rotor is presented in Figure 2.3. The terms dq and  $\alpha\beta$  represent the synchronous and space vector coordinates respectively. The q-axis is placed orthogonally to the d-axis, which is aligned with the flux vector caused by the PMs. The region between the rotor and stator is known as the air gap. In Figure 2.3, the rotor angle  $\vartheta_m$ , in terms of the electrical angular rotor speed  $\omega_m$  is given as

$$\omega_m = \frac{d\vartheta_m}{dt} \quad (2.9)$$

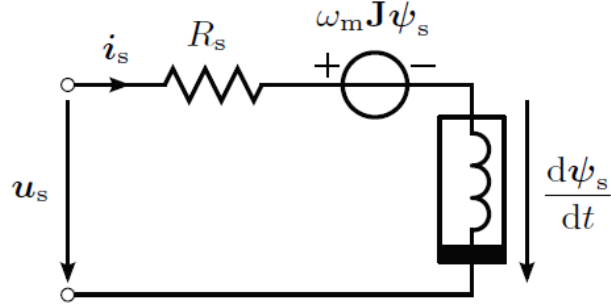


Figure 2.4: Dynamic space vector model of PM-SyRMs in rotor coordinates. [16]

The dynamic space vector model of PM-SyRMs in rotor coordinates is presented in Figure 2.4. Without the presence of PMs, PM-SyRMs are reduced to SyRMs, so by modelling a PM-SyRM and simply removing the PM flux term we get the magnetic model of SyRMs. For the modelling purposes of PM-SyRMs, real space vectors will be used instead of the complex space vectors. In terms of rotor coordinates, the stator voltage equation is given by

$$\mathbf{u}_s = R_s \mathbf{i}_s + \frac{d\boldsymbol{\psi}_s}{dt} + \omega_m \mathbf{J} \boldsymbol{\psi}_s \quad (2.10)$$

where  $\mathbf{u}_s$  is the stator voltage,  $\mathbf{i}_s$  is the stator current,  $\boldsymbol{\psi}_s$  is the stator flux and  $R_s$  represents the stator resistance. The real space vectors  $\mathbf{u}_s$ ,  $\mathbf{i}_s$ , and  $\boldsymbol{\psi}_s$  are given as

$$\mathbf{u}_s = \begin{bmatrix} u_d \\ u_q \end{bmatrix}, \quad \mathbf{i}_s = \begin{bmatrix} i_d \\ i_q \end{bmatrix}, \quad \boldsymbol{\psi}_s = \begin{bmatrix} \psi_d \\ \psi_q \end{bmatrix} \quad (2.11)$$

The stator voltage equation (2.10) in component form can be written as

$$u_d = R_s i_d - \omega_m \psi_q + \frac{d\psi_d}{dt} \quad (2.12a)$$

$$u_q = R_s i_q + \omega_m \psi_d + \frac{d\psi_q}{dt} \quad (2.12b)$$

For non-linear SMs, the flux linkages in terms of the motor currents can be represented as

$$\psi_d = \psi_d(i_d, i_q) \quad (2.13a)$$

$$\psi_q = \psi_q(i_d, i_q) \quad (2.13b)$$

Using (2.13), the motor inductances of non-linear SMs, in component form can be represented as

$$L_d(i_d, i_q) = \frac{\psi_d(i_d, i_q)}{i_d} \quad (2.14a)$$

$$L_q(i_d, i_q) = \frac{\psi_q(i_d, i_q)}{i_q} \quad (2.14b)$$

On the other hand, when PMSMs exhibit linear behaviour and the inductance values remain constant, the stator flux can be represented as

$$\boldsymbol{\psi}_s = \mathbf{L}_s \mathbf{i}_s + \boldsymbol{\psi}_{\text{pm}} \quad (2.15)$$

where  $\mathbf{L}_s$  represents the inductance matrix in rotor coordinates and  $\boldsymbol{\psi}_{\text{pm}}$  indicates the real space vector of the stator flux caused by the PMs. The matrices  $\mathbf{L}_s$  and  $\boldsymbol{\psi}_{\text{pm}}$  are given as

$$\mathbf{L}_s = \begin{bmatrix} L_d & 0 \\ 0 & L_q \end{bmatrix}, \quad \boldsymbol{\psi}_{\text{pm}} = \begin{bmatrix} \psi_{\text{pm}} \\ 0 \end{bmatrix} \quad (2.16)$$

In (2.12), for constant inductance values, the stator flux  $\boldsymbol{\psi}_s$  in component form is given as

$$\psi_d = L_d i_d + \psi_{\text{pm}} \quad (2.17a)$$

$$\psi_q = L_q i_q \quad (2.17b)$$

For SyRMs, the d-axis is aligned along the maximum inductance axis. In order to obtain the model of SyRMs, the PM flux term  $\psi_{\text{pm}}$  is eliminated ( $\psi_{\text{pm}} = 0$ ) from (2.17). On the other hand, if  $L_d = L_q = L_s$  is substituted in (2.17), we get the magnetic model for SPMs. The magnitude of the stator voltage, current and flux vectors are given as

$$u_s = \sqrt{u_d^2 + u_q^2} \quad (2.18a)$$

$$i_s = \sqrt{i_d^2 + i_q^2} \quad (2.18b)$$

$$\psi_s = \sqrt{\psi_d^2 + \psi_q^2} \quad (2.18c)$$

## 2.4 Saturation

In SMs, the flux linkages are produced as a result of the magnetic field created by the motor currents but the core of the motor can tolerate a specific amount of flux production beyond which it begins to saturate, this phenomenon is known as saturation. Saturation effects are significant for all types of SMs as they have a major impact in defining the characteristics of the motor. In PMSMs, the flux produced by PMs affects the inductances which also contributes to the saturation phenomenon. In SyRMs and PM-SyRMs, the flux linkages pass in parts through the rotor core due to which the motor inductances become dependant on the cross axis current alongside with the self axis current [17]. The saturation caused by this process is known as cross saturation. In cross saturation, the increase in either of the d- or q-axis current makes the flux linkage in the opposite axis to saturate.

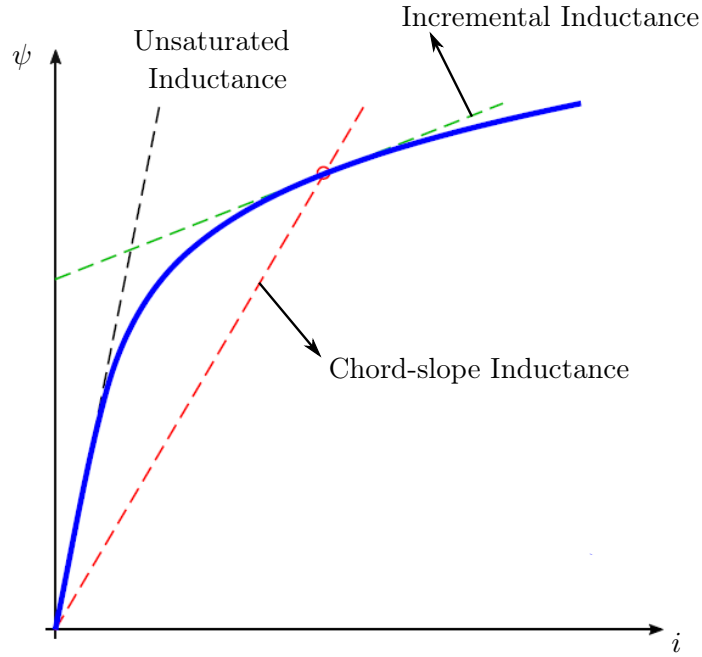


Figure 2.5: Saturation curve  $\psi = \psi(i)$ .

The motor inductance can be defined in various ways with respect to the non linear behaviour of different SMs. Since, the orientation of the d- and q-axis varies for different types of SMs, a general saturation curve is shown in Figure 2.5, where the flux linkage is taken as a function of current. Depending upon the value of inductance, the saturation curve can be divided into three regions. In Figure 2.5, the first region is known as the unsaturated region, where the relationship between the flux and current is linear. In the unsaturated region, the inductance value remain at its unsaturated nominal value. Referring to Figure 2.5, the chord-slope inductance is present in the second region, which is given as

$$L(i) = \frac{\psi(i)}{i} \quad (2.19)$$

The third region represents the incremental inductance, which is given as the ratio between the rate of change of flux and the rate of change of current. In Figure 2.5, the incremental inductance is given as

$$L_i(i) = \frac{\partial \psi(i)}{\partial i} \quad (2.20)$$

In the saturation curve shown in Figure 2.5, the current ( $i$ ) is an independent variable which is difficult to model with simple algebraic models. In order to make the modelling process simpler, the incremental inductance from the stator voltage equation can be excluded by taking the motor current as a nonlinear function of flux.

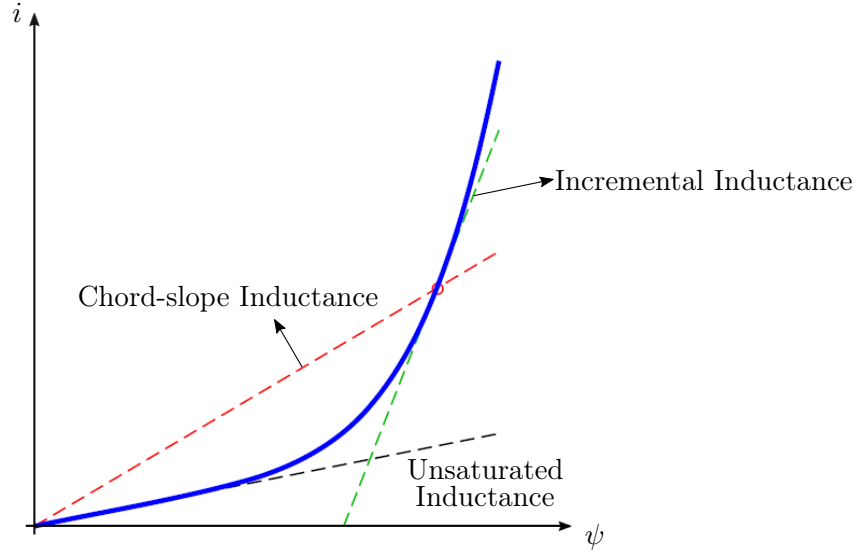


Figure 2.6: Saturation curve  $i = i(\psi)$ .

The saturation curve  $\psi = \psi(i)$ , in inverted coordinates, is presented in Figure 2.6, where the motor current is taken as a function of flux linkage  $i = i(\psi)$ .

The motor currents in terms of the motor flux linkages are given as

$$i_d = i_d(\psi_d, \psi_q) \quad (2.21a)$$

$$i_q = i_q(\psi_d, \psi_q) \quad (2.21b)$$

## 2.5 Torque Generation in Synchronous Motors

The electromagnetic torque of IPMs in rotor synchronous coordinates is given as

$$T_e = \frac{3p}{2}(\psi_d i_q - \psi_q i_d) \quad (2.22)$$

where  $p$  represents the number of pole pairs of the motor. By considering (2.17), the torque equation of IPMs in terms of the motor inductances can be written as

$$T_e = \frac{3p}{2}[\psi_{pm} + (L_d - L_q)i_d]i_q \quad (2.23)$$

By replacing  $L_d = L_q$  in (2.23), the electromagnetic torque of SPMs is obtained

$$T_e = \frac{3p}{2}\psi_{pm}i_q \quad (2.24)$$

In case of SyRMs, by substituting  $\psi_{\text{pm}} = 0$  in (2.23), the torque equation is given as

$$T_e = \frac{3p}{2}(L_d - L_q)i_d i_q \quad (2.25)$$

In (2.23) and (2.25), the reluctance torque, represented by the term  $\frac{3p}{2}(L_d - L_q)i_d i_q$  is generated due to the salient structure of IPMs and SyRMs. For SyRMs, if  $L_d > L_q$ , the production of the torque can be increased by using positive values of the d-axis current. While, for PM-SyRMs and IPMs when ( $L_d < L_q$ ), the torque production can be increased by using negative values of  $i_d$ .

## 3 Identification Techniques

The experimental magnetic model identification methods for SMs can be broadly divided into standstill and constant speed methods. Experimental magnetic model identification methods are useful when only the rated motor data is available and no other information is known. There are various advantages of effectively identifying the magnetic model of synchronous motors such as

- The magnetic model identification helps in the determination of different control trajectories like the maximum torque per ampere (MTPA) and maximum torque per volt (MTPV), which are necessary for the complete utilization of the motor speed and torque range [4].
- The information about the motor design and manufacturing is not required for the purpose of making comparisons between different motors produced by various manufacturers [4].

The magnetic model identification is important for the complete and accurate assessment of any motor. In this chapter, numerous standstill and constant speed experimental methods used for the magnetic model identification of SMs have been reviewed in detail.

### 3.1 Standstill Identification Methods

The standstill identification methods can be divided into two categories, the first one with locked rotor and the other with unlocked rotors [5, 18]. The knowledge of the position of the motor is required in some cases whereas various sensorless methods have also been presented [18, 19]. Vector current control scheme is used to identify the magnetic model of various motors at standstill conditions. For an IPM, with the rotor position locked, a step voltage pulse using a voltage source inverter is applied to the motor while the motor is controlled through constant current [5]. For the estimation of the flux linkages in the self and cross-saturation condition, voltage pulses are applied simultaneously to the motor d-and q-axis.

For self and cross-saturation, the variations in the flux linkages corresponding to the motor currents are required for estimating the motor inductances. To identify the flux linkage in q-axis, the current is kept constant in the d-axis while a voltage pulse is applied in the q-axis [5]. The magnitude of the applied voltage,  $u_q$  is kept high enough so that the corresponding current  $i_q$ , covers the full operating range of the motor.

The q-axis flux linkage is then evaluated by solving the stator voltage equation over a certain time duration

$$\psi_q(t) = \int \{u_q(t) - R_s i_q(t)\} dt \quad (3.1)$$

In a similar manner, to estimate the d-axis flux linkage, a voltage pulse is applied in the d-axis while the motor is controlled by the constant current in the q-axis. This process only evaluates the armature flux linkage in the d- and q-axis which is later combined with the PM flux linkage  $\psi_{pm}$  calculated from the open circuit test to complete the motor model [3]. In the open circuit test, motor voltages are measured at constant speed to find the PM flux linkage. In steady state, for every value of the voltage pulse, the stator resistance can be estimated as the ratio between the stator voltage and current. The major drawback of this method is the low accuracy of the estimated flux linkages. For the motor to operate in the steady state, the values of the applied voltage pulses are kept low which makes the resultant flux linkage largely dependent upon the inverter voltage and stator resistance [18].

## 3.2 Self-Commissioning Techniques

Self-commissioning techniques can be helpful for the drive users in assessing and controlling various parameters which can be used for the control of motors that come without any valuable information. Since last few years, various self-commissioning methods for SMs have been presented [18–21]. Some self-commissioning methods for SMs, that does not require any additional features other than the standard setup required for operating different SM drives have been discussed in the following subsections

### 3.2.1 Self-Commissioning at Standstill Conditions

A lot of research has been going on for the sensorless self-commissioning of IPMs and SyRMs at standstill conditions, various methods have been presented in the literature [18, 19, 22]. With the rotor unlocked, bipolar voltage pulses are applied to a SyRM with the help of an inverter and the flux linkages are calculated with the help of the voltage induced in the stator [18, 19].

For a SyRM, with the rotor kept unlocked, the d- and q-axis flux linkages are estimated by considering both the self and cross-saturation conditions [18]. The initial rotor position can be determined before the experiment either by using the signal injection method or by parking the rotor in the required direction by applying the DC current to the motor [18]. In order to estimate the q-axis flux linkage, voltage in the q-axis is varied in steps with the d-axis voltage kept at zero.

The current is controlled by using a hysteresis controller and its value is limited by defining a maximum current value. With the reference voltage in the d-axis equal

to zero, the control rule used for generating the q-axis test voltage in the hysteresis controller is given as [18]:

$$u_{q,\text{ref}}(k) = \begin{cases} u_{q,\text{out}} & \text{for } i_q(k) < -i_{q,\text{max}} \\ -u_{q,\text{out}} & \text{for } i_q(k) > i_{q,\text{max}} \\ u_{q,\text{ref}}(k-1) & \text{elsewise} \end{cases}$$

where  $k$  represents the discrete-time index, the magnitude of the test voltage is given by  $u_{q,\text{ref}}$  while  $i_{q,\text{max}}$  denotes the current limit for which the flux linkages are identified. The value of  $i_{q,\text{max}}$  should be chosen low enough to eliminate any possible rotor movement.

In case of the d-axis, similar type of control law is used to generate the d-axis test voltages for which the d-axis flux linkages are evaluated. For the cross saturation condition, the voltage pulses are applied simultaneously to the d- and q-axis of the motor and the corresponding measurements are used to calculate the flux linkages. The magnitude of the applied voltage pulses is kept around the rated motor voltage which makes the flux estimation immune to the stator resistance and inverter voltage drop.

### 3.2.2 Self-Commissioning at Free Shaft

For PMSMs, a self-commissioning method at free shaft has been presented in [22]. With the machine shaft free to rotate, the current of the test machine is controlled for the evaluation of the dq-axis flux linkages. The d- and q-axis reference currents are varied in a suitable manner so that the test machines covers both the positive and negative speed operating regions [22]. The test machine shaft is kept detached from any kind of non interial load. At first, positive d- and q-axis reference currents are supplied to the current vector controller, which results in the acceleration of the machine. Then, positive d- and negative q-axis reference currents are supplied to the current vector controller, which results in the deceleration of the machine. The flux linkages for the acceleration and deceleration condition are estimated from the steady state stator voltage equation.

The stator resistance  $R_s$  must be estimated before starting the experiment by taking into account the motor temperature so the correct value of  $R_s$  is used during the experiment [22]. A position sensor is mounted on the test machine shaft to get information regarding the variable rotor speed ( $\omega_m$ ) while voltage commands are used to get the voltage vectors required for the flux linkages estimation [21,23]. Finally, the machine flux linkages are evaluated, by taking the average of the acceleration and deceleration conditions. The flux linkage estimation is given as

$$\psi_d = \frac{\psi_{d,m} + \psi_{d,b}}{2}, \quad \psi_q = \frac{\psi_{q,m} - \psi_{q,b}}{2} \quad (3.2)$$

where the subscripts  $\psi_{d,m}$  and  $\psi_{q,m}$  represents the flux linkages estimated during acceleration and  $\psi_{d,b}$  and  $\psi_{q,b}$  represents the flux linkages estimated during deceleration.

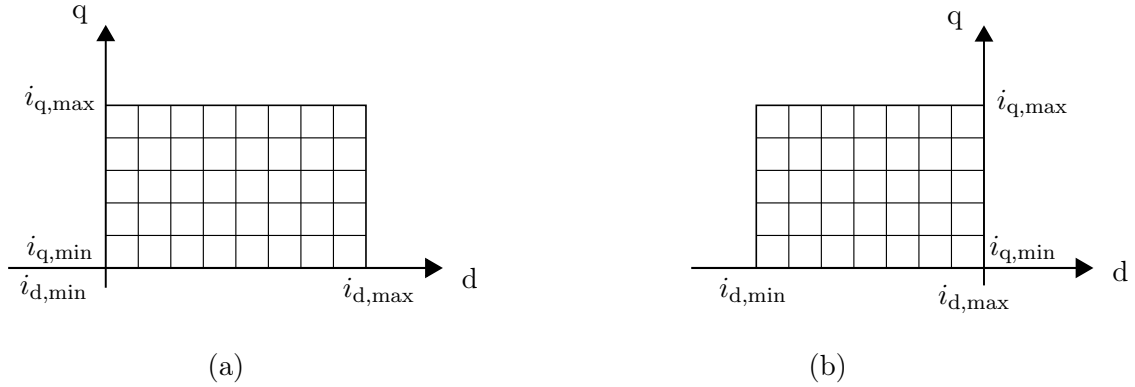


Figure 3.1: Current grids for SyRMs and PMSMs.

### 3.3 Constant Speed Identification Methods

Alongside standstill identification methods, various constant speed magnetic model identification techniques of SMs have also been proposed [4, 11]. In [11], constant (dq) current components are applied to the test motor and the output voltage components are measured. A low pass filter and fast Fourier transform are used to extract the fundamentals components of the output voltage, for the evaluation of flux linkages. The stator resistance variation alongside iron losses are not compensated in [11], which makes the flux linkage identification inaccurate for high speed levels.

In steady state conditions, for a SyRM and PM-SyRM running at constant speed, by controlling the d- and q-axis currents and measuring the corresponding voltages, the flux linkages are identified [4]. The variation in the stator resistance is compensated which makes the magnetic model identification possible for any current level whereas other factors such as the iron losses and voltage harmonics are also taken into consideration [4]. The dq-axis flux linkages evaluated as a function of the motor currents are given as

$$\psi_d = \psi_d(i_d, i_q) \quad (3.3a)$$

$$\psi_q = \psi_q(i_d, i_q) \quad (3.3b)$$

The flux linkages are evaluated in a rectangular area between the points  $i_{d,\min} \rightarrow i_{d,\max}$  and  $i_{q,\min} \rightarrow i_{q,\max}$  on the d- and q-axis of the current plane as shown in Figure 3.1. The d- and q-axis current sequences are generated by equivalent spaced array which are given as [4]

$$i_{d,k} = i_{d,\min} + k \Delta i_d \quad k = 1, 2, 3. \quad (3.4a)$$

$$i_{q,k} = i_{q,\min} + n \Delta i_q \quad n = 1, 2, 3. \quad (3.4b)$$

where  $\Delta i_d$  and  $\Delta i_q$  represent the value of the step change that occurs in  $i_d$  and  $i_q$ .

For SyRMs, the flux linkages are identified by using equally spaced positive arrays of the d- and q-axis currents as given in Figure 3.1 (a) [4]. In case of PMSMs, negative values of  $i_d$  and positive values of  $i_q$  can be used for identification purposes as shown in Figure 3.1 (b).

In steady state, the voltage equation (2.12) in component form is given as

$$u_d = R_s i_d - \omega_m \psi_q \quad (3.5a)$$

$$u_q = R_s i_q + \omega_m \psi_d \quad (3.5b)$$

From (3.5), the d- and q-axis flux linkages can be calculated as

$$\psi_d = \frac{u_q - R_s i_q}{\omega_m} \quad (3.6a)$$

$$\psi_q = - \left( \frac{u_d - R_s i_d}{\omega_m} \right) \quad (3.6b)$$

Using (3.6), various values of flux linkages can be estimated by measuring the d- and q-axis voltages after applying different values of  $i_d$  and  $i_q$ . But in (3.6), the variation in the stator resistance can reduce the accuracy of the estimated flux linkages. In order to remove the impact of stator resistance, initially the motor is run in the motoring mode by applying positive d- and q-axis current ( $+i_d, +i_q$ ) for which the output voltages are measured [4]. Immediately, the motor is run in the generating mode by applying positive d-axis and negative q-axis current ( $+i_d, -i_q$ ) and again the output voltages are measured. After the motoring and generating conditions, some possible variation in the stator resistance still may occur which is accommodated, by again applying the motoring condition and measuring the output voltages [4]. The three current pulses combined, two in the motoring and one in the generating condition collectively gives a single flux linkage point. After applying the first motoring condition, the d- and q-axis flux linkages calculated from (3.6) are given as

$$\psi_{d1} = \frac{u_{q1} - R_s i_{q1}}{\omega_m} \quad (3.7a)$$

$$\psi_{q1} = - \left( \frac{u_{d1} - R_s i_{d1}}{\omega_m} \right) \quad (3.7b)$$

where  $u_{d1}, u_{q1}$  are the measured voltages in the first motoring condition whereas  $i_{d1}$  and  $i_{q1}$  are the currents supplied to operate the motor in motoring mode.

After the first motoring condition, the motor is run in the generating mode, for which the d- and q-axis flux linkages calculated using (3.6) are given as

$$\psi_{d2} = \frac{u_{q2} - R_s i_{q2}}{\omega_m} \quad (3.8a)$$

$$\psi_{q2} = - \left( \frac{u_{d2} - R_s i_{d2}}{\omega_m} \right) \quad (3.8b)$$

where  $u_{d2}$ ,  $u_{q2}$  are the measured voltages in the generating condition while  $i_{d2}$  and  $i_{q2}$  are the currents in the generating mode. In (3.8), the d-axis current  $i_{d2} = i_{d1}$  while the q-axis current  $i_{q2} = -i_{q1}$  because the reference current values remain the same during the motoring and generating mode.

Finally, the motor is run again in the motoring mode to eliminate any possible resistance variation that may still be present. By using (3.6), the d- and q-axis flux linkages calculated for the second motoring condition are given as

$$\psi_{d3} = \frac{u_{q3} - R_s i_{q3}}{\omega_m} \quad (3.9a)$$

$$\psi_{q3} = -\left(\frac{u_{d3} - R_s i_{d3}}{\omega_m}\right) \quad (3.9b)$$

where  $u_{q3}$ ,  $u_{d3}$  are the voltages measured in the second motoring condition whereas  $i_{d2}$  and  $i_{q3}$  are the currents during the second motoring mode. In (3.9), the d-axis current  $i_{d3} = i_{d1}$  while the q-axis current  $i_{q3} = i_{q1}$ , as the reference current value remains the same for a single flux linkage point calculation.

In order to calculate a single d- and q-axis flux linkage point, the average of the flux linkages calculated in the motoring and generating mode is taken

$$\psi_d = \frac{1}{2} - \left(\frac{\psi_{d1} + \psi_{d3}}{2} + \psi_{d2}\right) \quad (3.10a)$$

$$\psi_q = \frac{1}{2} - \left(\frac{\psi_{q1} + \psi_{q3}}{2} - \psi_{q2}\right) \quad (3.10b)$$

where  $\psi_{d1}$ ,  $\psi_{d3}$ ,  $\psi_{q1}$ ,  $\psi_{q3}$  represent the flux linkages calculated in the motoring modes and  $\psi_{d2}$ ,  $\psi_{q2}$  are the flux linkages calculated in the generating mode. In the generating mode,  $i_{q2}$  is negative due to which the corresponding flux  $\psi_{q2}$  is negative. By replacing the values of  $\psi_{d1}$ ,  $\psi_{d2}$ ,  $\psi_{d3}$  in (3.10a), the d-axis flux linkage is given as

$$\psi_d = \frac{1}{2} - \left(\frac{u_{q1} + u_{q3}}{2} - R_s i_{q1} + u_{q2} + R_s i_{q1}\right) \frac{1}{\omega_m} \quad (3.11)$$

From (3.11), it can be seen that terms containing the stator resistance cancel out each other and the resultant d-axis flux linkage becomes independent of the stator resistance. With the motor running at constant speed, a single d-axis flux linkage point calculated from the motoring and generating conditions is given as

$$\psi_d = \frac{1}{2} \left(\frac{u_{q1} + u_{q3}}{2} + u_{q2}\right) \frac{1}{\omega_m} \quad (3.12)$$

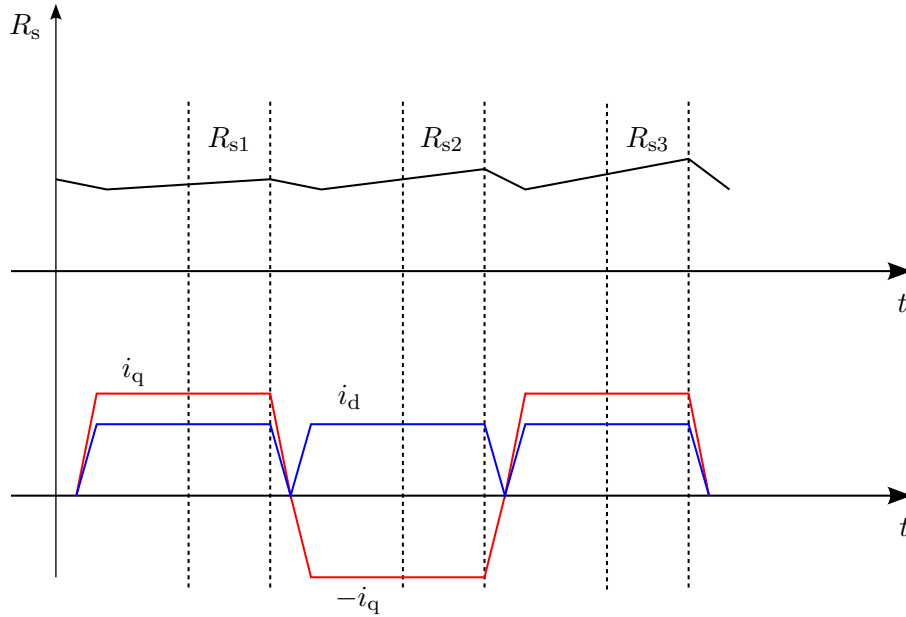


Figure 3.2: Deviation in  $R_s$  due to temperature variation during the motoring and generating conditions.

Similarly, by replacing the values of  $\psi_{q1}$ ,  $\psi_{q2}$ ,  $\psi_{q3}$  in (3.10b), the q-axis flux linkage is given as

$$\psi_d = \frac{1}{2} - \left( \frac{u_{q1} + u_{q3}}{2} - R_s i_{d1} + u_{q2} + R_s i_{d1} \right) \frac{1}{\omega_m} \quad (3.13)$$

From (3.13), it is clear that the resultant q-axis flux linkage is also independent of the stator resistance. At constant motor speed, a single q-axis flux linkage point calculated from the motoring and generating conditions is given as

$$\psi_q = -\frac{1}{2} \left( \frac{u_{d1} + u_{d3}}{2} - u_{d2} \right) \frac{1}{\omega_m} \quad (3.14)$$

Along with the stator resistance, the errors due to the fundamental components of the dead time voltage errors and inverter voltage are also removed when the average of the measured voltages is taken [4]. By applying different current values to the motor and measuring the corresponding voltages, look-up tables can be formulated between the motor flux linkages and currents. By using these look-up tables, the flux maps can be defined in terms of motor currents.

In case of PMSMs, the temperature value may alter while applying the current pulses. If the temperature varies during the motoring and generating modes, the average temperature of the first and third pulses which are applied during the motoring conditions will be equal to the average temperature of the second pulse that is applied during the generating condition [4]. This average temperature value can be taken as the value of stator resistance as shown in Figure 3.2.

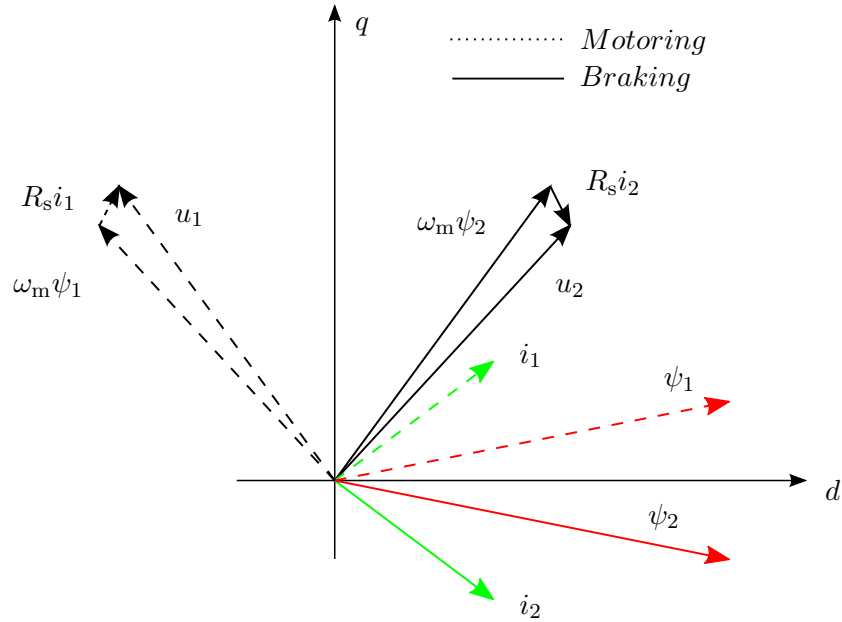


Figure 3.3: Voltage, current and flux linkage vector diagram of a SyRM.

In case of temperature variation, the stator resistance can be found as

$$R_s = \frac{R_{s1} + R_{s3}}{2} = R_{s3} \quad (3.15)$$

where  $R_{s1}$  and  $R_{s3}$  represent the stator resistance variation in the motoring conditions while  $R_{s2}$  is the stator resistance variation in the generating condition that occur due to the temperature variation in the current pulses.

Figure 3.3 represents the voltage, current and flux linkage vector diagram of a SyRM without the presence of the iron losses. It can be seen that the conjugate current vectors  $i_1$  and  $i_2$  result in two flux linkage vectors given by  $\psi_1$  and  $\psi_2$  whereas the corresponding voltage vectors  $u_1$  and  $u_2$  differ in terms of the voltage drop across the stator resistance. The subscript 1 represents the motoring condition while the subscript 2 represents the generating condition.

When the core losses are taken into consideration, while applying the motoring and generating conditions, the current vectors remain the conjugate of each other but the flux linkages no longer remain the conjugates because of the current component ( $i_{fe}$ ) produced by the core losses. The steady state vector diagram of a SyRM, with the presence of iron losses is given by Figure 3.4.

The selection of the correct speed level is of essential importance as the iron losses depend on it. For the voltage measurement, the rotor speed is needed to be high enough to produce high levels of the d- and q-axis voltages with high signal to noise ratio. On the contrary, the speed should be low enough to reduce the impact of the iron losses on the identification process. One third value of the base speed is a good trade off between the iron losses and high output voltage levels [4].



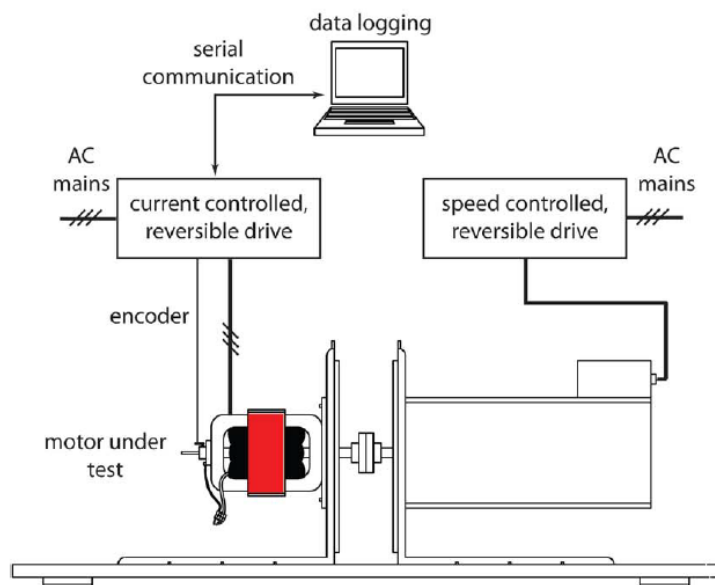


Figure 3.5: Experimental setup containing a test motor and a servo motor drive [4].

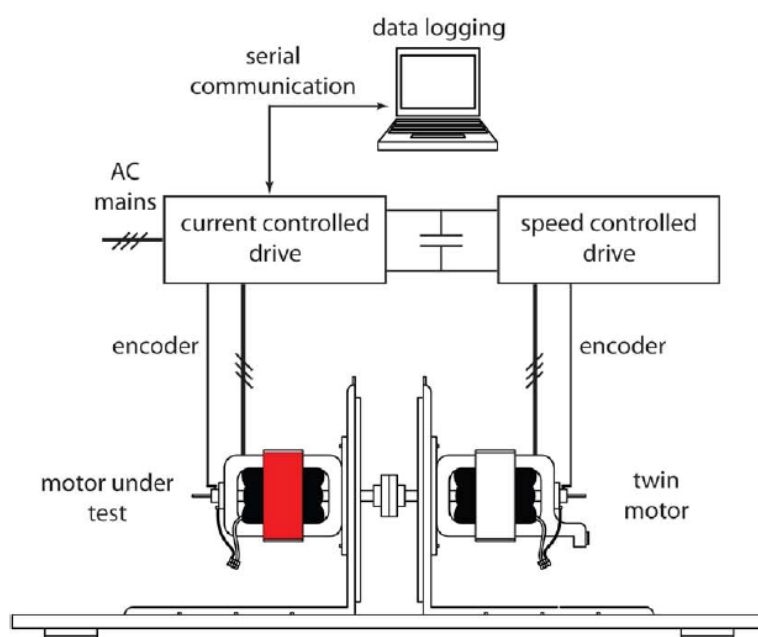
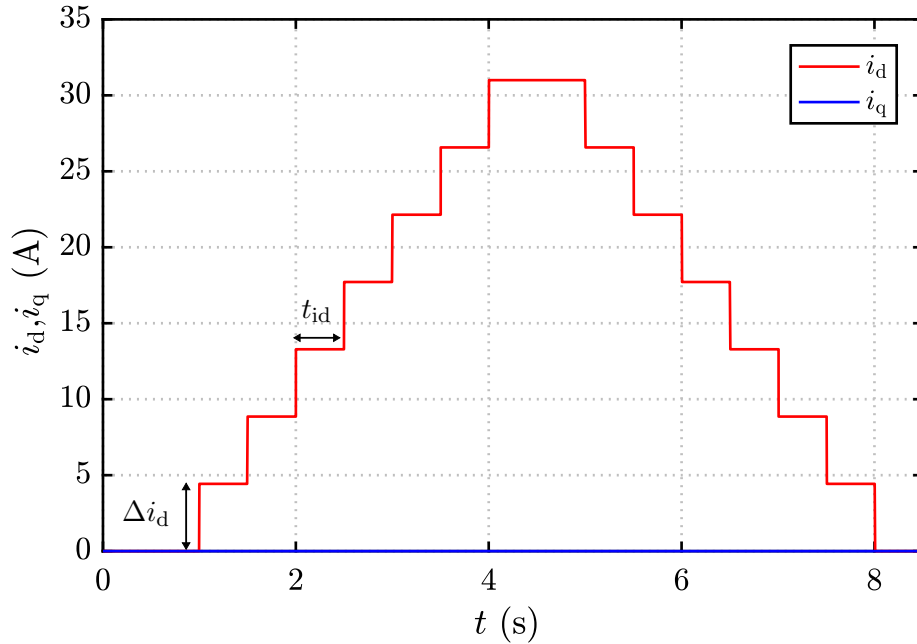


Figure 3.6: Experimental setup consisting of duplicate electric drives and two test motors [4].

as represented in Figure 3.6. The benefit of this arrangement is that it does not require any four quadrant drives like the first setup.

Table 3.1: Parameters used in reference current generation.

Number of steps in $i_{d,\text{ref}}$	$N_d$
Number of steps in $i_{q,\text{ref}}$	$N_q$
Maximum d-axis current	$i_{d,\text{max}}$
Maximum q-axis current	$i_{q,\text{max}}$
Time before step change	$t_{id}$

Figure 3.7: Reference d-axis current generation limited by  $i_{d,\text{max}}$ 

### 3.4 Reference Current Generation

The magnetic model identification technique presented in [4] for the evaluation of the flux linkages is taken as reference for the generation of the current sequence. The d- and q-axis reference currents are generated by taking into account the motoring and generating phenomenon. The parameters used during the reference current generation are presented in Table 3.1. The d-axis reference current  $i_{d,\text{ref}}$  is generated in a step-wise manner limited by the maximum current  $i_{d,\text{max}}$ , where  $N_d$  represents the number of steps required to reach  $i_{d,\text{max}}$ . The value of the step change is represented by  $\Delta i_d$  which is given as  $\Delta i_d = \frac{i_{d,\text{max}}}{N_d}$ , while the time duration after which the step change occurs is denoted by  $t_{id}$ .

Initially,  $i_{d,\text{ref}}$  is increased in steps until the maximum current limit is reached. When the maximum current limit  $i_{d,\text{max}}$  is reached,  $i_{d,\text{ref}}$  is decreased in a step-wise manner until zero reference current is reached. One complete cycle showing the step-wise increase and decrease in  $i_{d,\text{ref}}$  with zero reference current in the q-axis is shown in Figure 3.7.

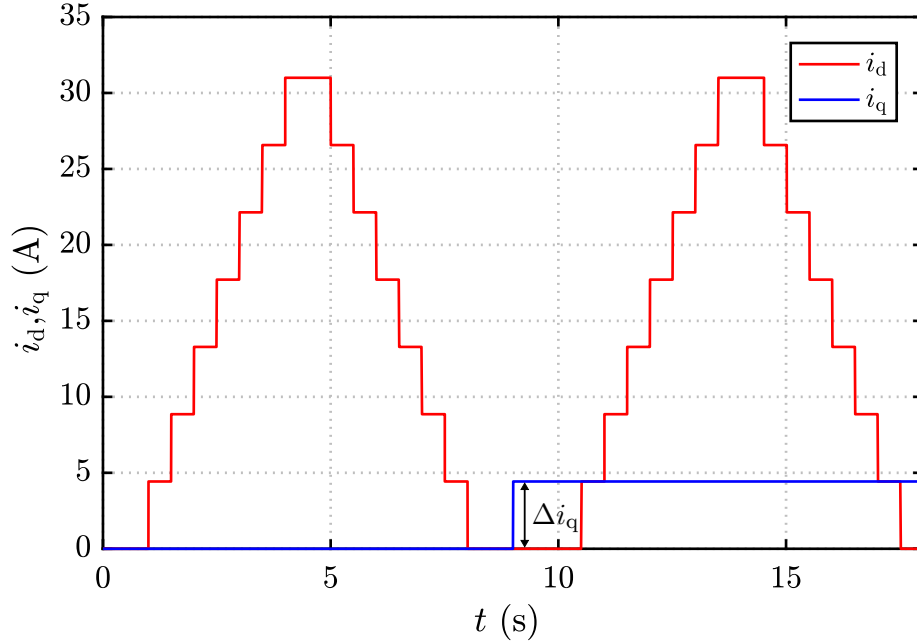


Figure 3.8: Reference current generation for motoring mode ( $i_{d,\text{ref}}, i_{q,\text{ref}}$ )

The q-axis reference current  $i_{q,\text{ref}}$  is generated by considering the motoring and generating conditions. For the motoring mode,  $i_{q,\text{ref}}$  has positive values that are limited by the maximum current  $i_{q,\text{max}}$ . The value of the step change is represented by  $\Delta i_q$  which is given as  $\Delta i_q = \frac{i_{q,\text{max}}}{N_q}$ , while the time duration after which the step change occurs is defined by  $t_{id}$ . Figure 3.8 illustrates the first motoring condition, where the reference currents  $i_{d,\text{ref}}$  and  $i_{q,\text{ref}}$  have positive values.

When the second sequence of  $i_{d,\text{ref}}$  is completed and the condition  $i_{d,\text{ref}} = 0$  is reached, the value of  $i_{q,\text{ref}}$  is flipped to  $-i_{q,\text{ref}}$ . Figure 3.9 illustrates the generating condition, where  $i_{d,\text{ref}}$  has positive values and  $i_{q,\text{ref}}$  has negative values.

For calculating a single flux linkage point, two current pulses in motoring mode and one current pulse in generating mode is required. Figure 3.10 illustrates the second motoring condition, where the d- and q-axis reference currents have positive values. When the third sequence of  $i_{d,\text{ref}}$  is finished and the condition  $i_{d,\text{ref}} = 0$  is reached, the reference current  $-(i_{q,\text{ref}})$  is flipped again to  $+(i_{q,\text{ref}})$ . When the two motoring modes and one generating mode is completed, a single d- and q-axis flux linkage can be calculated from (3.11) and (3.13). In order to form look up tables between the flux linkages and motor currents, the current sequence can be continued to run by defining the maximum current limit. After the second motoring mode, the cycle of two motoring and one generating condition is repeated until the maximum current limit is reached. When the fourth sequence of  $i_{d,\text{ref}}$  is finished and the condition  $i_{d,\text{ref}} = 0$  is reached, the value of  $i_{q,\text{ref}}$  is changed to  $i_{q,\text{ref}} + \Delta i_q$ . Figure 3.11 illustrates the motoring condition for the next flux linkage point calculation, where  $i_{d,\text{ref}}$  and  $i_{q,\text{ref}}$  have positive values.

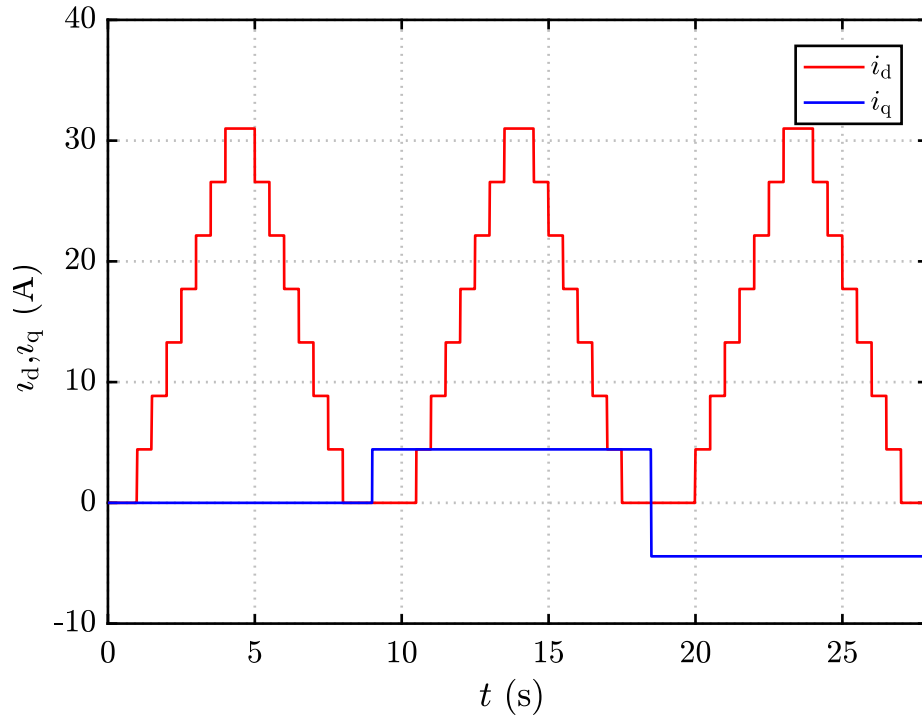


Figure 3.9: Reference current generation for the generating mode ( $i_{d,\text{ref}}, -i_{q,\text{ref}}$ )

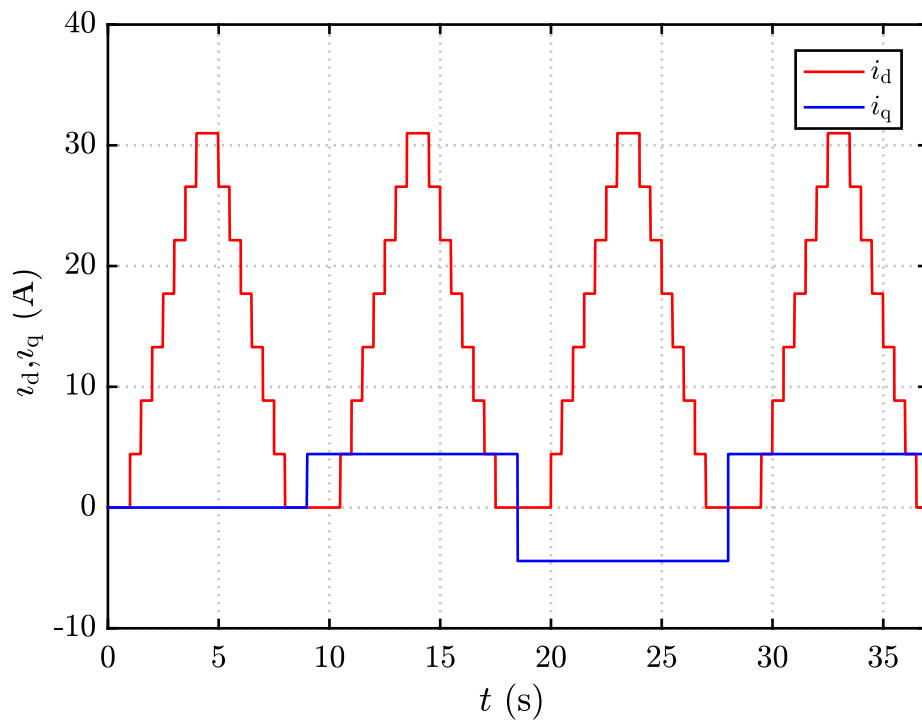


Figure 3.10: Reference current generation for the second motoring condition ( $i_{d,\text{ref}}, i_{q,\text{ref}}$ ).

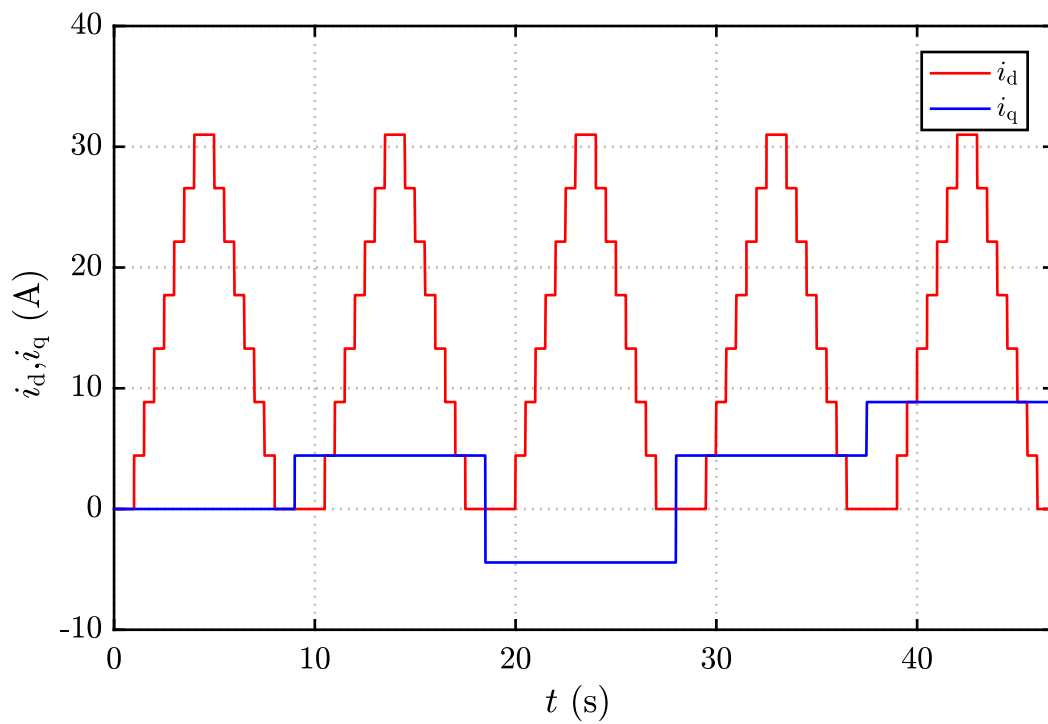


Figure 3.11: Step change in  $i_{q,\text{ref}}$  for repeating the motoring and generating conditions.  $(i_{d,\text{ref}}, i_{q,\text{ref}} + \Delta i_q)$

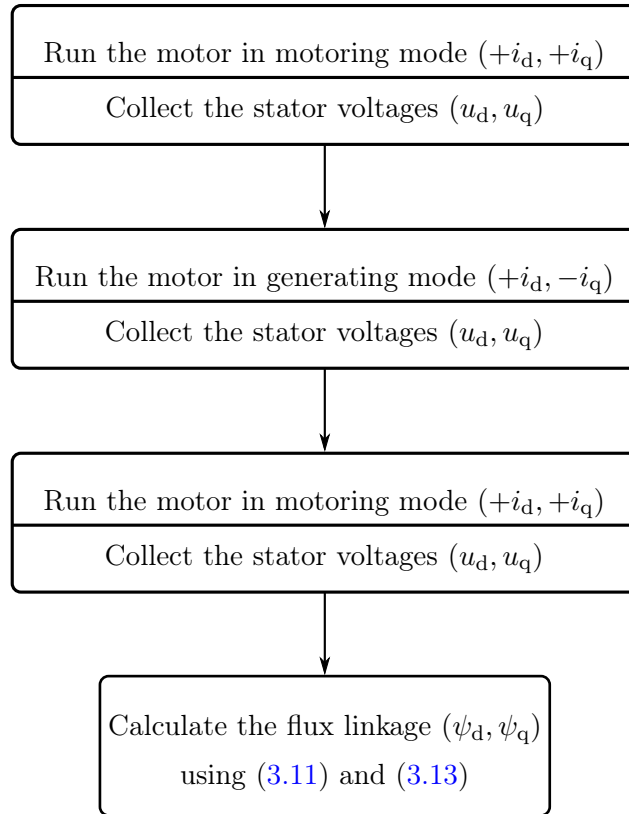


Figure 3.12: Flow diagram for a single flux linkage point calculation.

### 3.5 Flux Map Calculation

For the flux map calculations, the magnetic model identification method presented in [4] is taken as a reference. The flow diagram for calculating a single flux linkage point is shown in Figure 3.12. The reference current sequence mentioned in 3.4, can be used to identify any number of flux linkage points by defining the range of the maximum current values. The reference current sequence will keep on repeating the motoring and generating conditions until the maximum current value is reached, by calculating the corresponding output voltages, the d- and q-axis flux linkages can be determined using 3.11 and 3.13. From these calculated flux linkages, look-up tables can be formulated in terms of the motor currents. Once the relationship of the flux linkages related to the motor current is known, information regarding the motor inductances can be deduced which can be used to the saturation characteristic of a motor. A sample current sequence consisting of the repeating motoring and generating conditions that can be fed to the current controller, for calculating various flux linkages is presented in Figure 3.13.

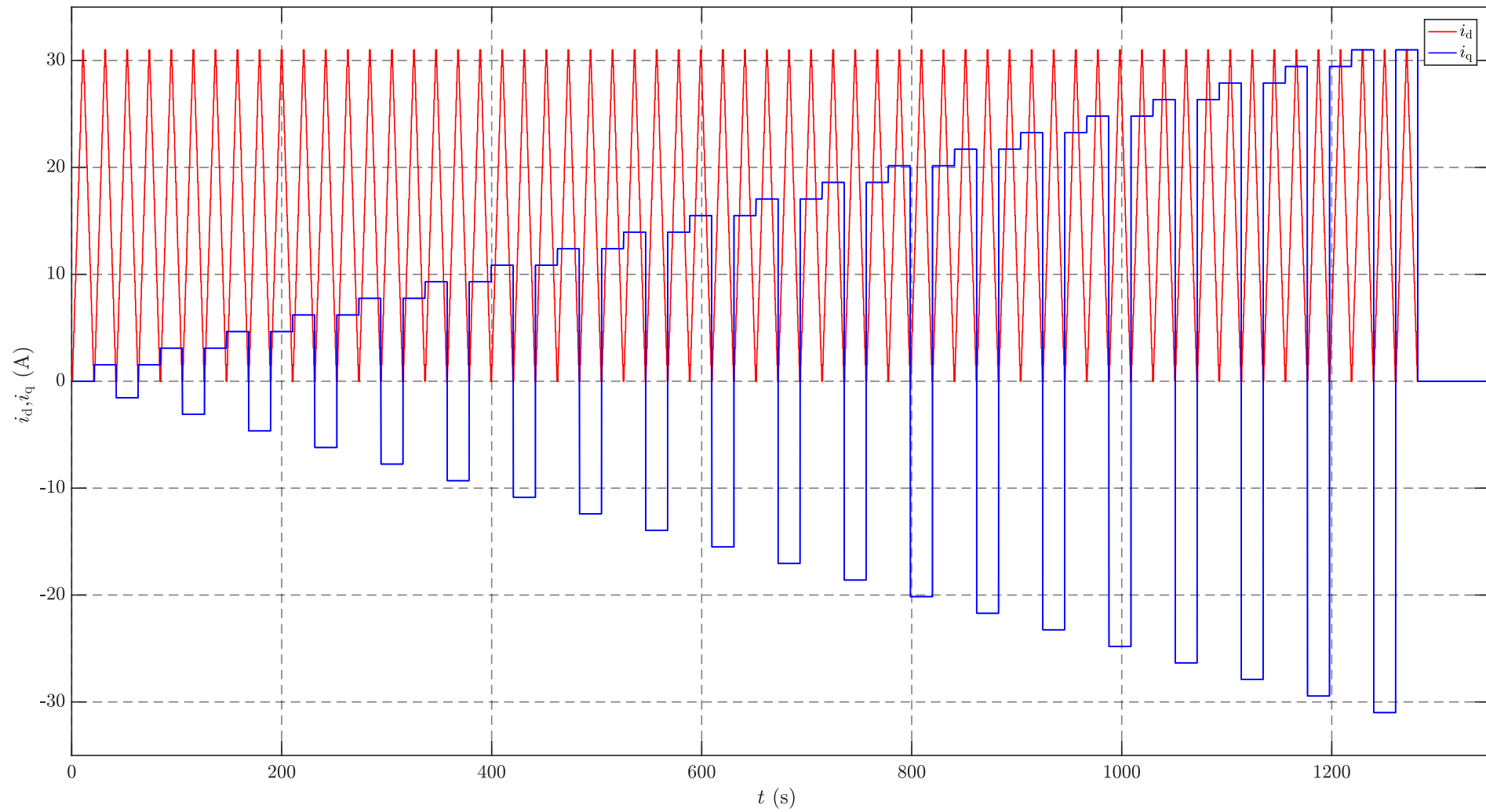


Figure 3.13: Sample reference current sequence.

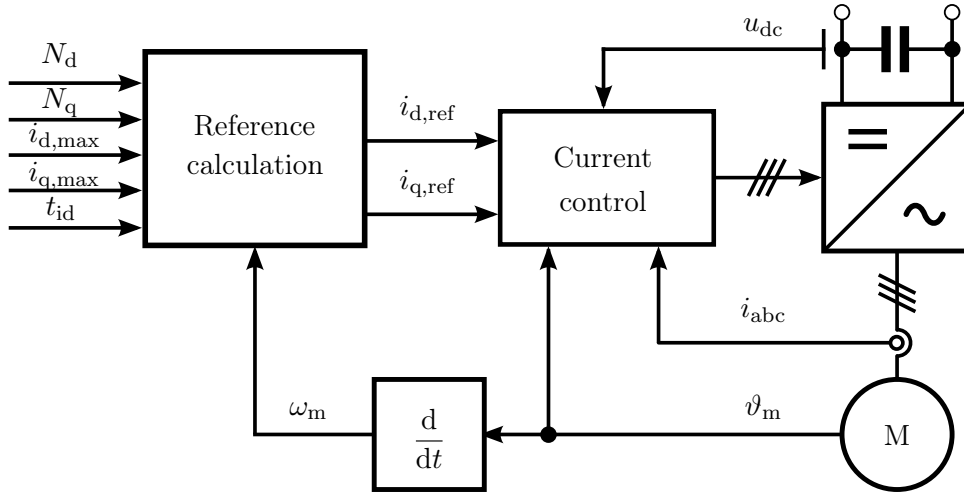


Figure 3.14: Flux linkage identification setup.

### 3.6 Current Controller

SMs are usually controlled through the vector control schemes. The vector control schemes, present the advantage to manipulate the torque as well as the flux of the synchronous motors by simply varying the d- and q-axis components of the stator current. Dynamic models of SMs are used to build the vector control schemes, for achieving high accuracy and quick dynamics in the motor performance. For some SMs, the knowledge about the rotor position is required in order to implement the vector control scheme that can be obtained by attaching a mechanical position sensor on the motor shaft.

Hysteresis controller, stator frame PI controller, state feedback controller, synchronous frame PI controller, dead-beat direct torque and predictive controllers are various types of controllers that can be used for the current control of synchronous motors [24, 25]. Hysteresis controller is the simplest controller in terms of implementation however unlike the synchronous frame PI controller, the switching frequency is not constant. The synchronous frame PI controller has a zero steady state error while the stator frame PI controller contains some steady state error. An integral action combined with the state feedback controller forms a special case of the synchronous frame PI controller.

Among these controllers, the synchronous frame PI controller designed with the help of internal model control (IMC) method can be regarded as a state-of-the-art controller. In this kind of controller, the motor model and desired controller bandwidth are used to determine the controller parameters such as the proportional and integral gain. The cross coupling present in the current components of the d- and q-axis is the major drawback that occur in the model based synchronous frame PI current controller. At any time, when a step change occurs in the reference value of the q-axis current, it yields a transient error in the d-axis current.

One step predicted current is one of the various suggestions that have been proposed to decrease the transient error in the model based synchronous frame PI controller [24]. The current components of the d- and q-axis contain high frequency oscillations throughout in steady state. By supplying one step predicted current into the decoupling and damping terms of the controller, these high frequency oscillations can be decreased.

In this thesis, the discrete-time state space controller with the integral action and state feedback as presented in [26] is used to control the d- and q-axis currents. The block diagram of the current controller with the reference current sequence generated for the flux linkage identification is presented in Figure 3.14.

## 4 Results

The results of this thesis are divided into three cases. The flux maps calculated for various values of the d- and q-axis currents are presented in case 1. In case 2, the d-axis flux linkage is calculated for the self and cross-saturation conditions by using the current values  $(0 \rightarrow i_{d,\max}, 0)$  and  $(0 \rightarrow i_{d,\max}, i_{q,\max})$  respectively. In case 3, the q-axis flux linkage is calculated for both the self and cross-saturation conditions by using the current values  $(0, 0 \rightarrow i_{q,\max})$  and  $(i_{d,\max}, 0 \rightarrow i_{q,\max})$  respectively. A four pole transverse-laminated 6.7-kW SyRM is used in the simulations whose rated values are given in Table 4.1. MATLAB/Simulink environment is used for the simulation purposes. The flux linkage look-up tables are used to calculate the flux maps for following conditions

- Case 1: The d-and q-axis flux linkages for various values of  $i_d$  and  $i_q$ .
- Case 2: The d-axis flux linkage in self and cross-saturation conditions.
- Case 3: The q-axis flux linkage in self and cross-saturation conditions.

The model of a 6.7-kW SyRM, presented in Figure 4.1 is used for the simulation purposes. The plant model “SyRM” is implemented in continuous time domain whereas the discrete-time-state-space current controller is used in the subsystem “Vector Control”. The motor speed alongside with the stator current are obtained through the output of the SyRM block. The rated values of the SyRM are given in Table 4.1 while the parameters used in simulation are given in Table 4.2.

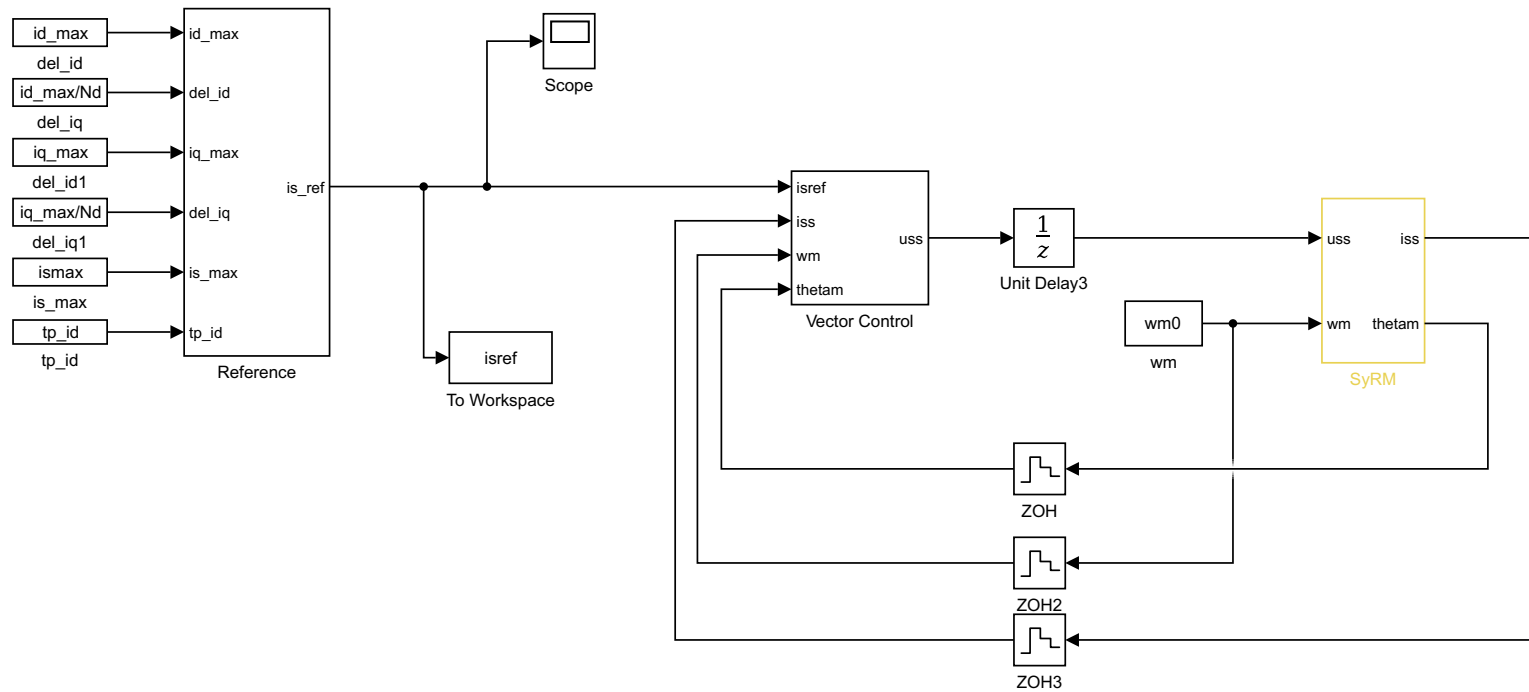


Figure 4.1: Simulation model of a SyRM.

Table 4.1: Ratings of the SyRM.

Rated power	$P_N$	6.7 kW
Rated voltage (rms L-L)	$U_N$	370 V
Rated current (rms)	$I_N$	15.5 A
Rated frequency	$f_N$	105.8 Hz
Rated torque	$T_N$	20.1 Nm
Rated speed	$\omega_m$	3175 r/min

Table 4.2: Parameters of the SyRM.

Stator resistance	$R_s$	0.55 $\Omega$
Pole pairs	$p$	2

## 4.1 Saturation Model

IPMs and SyRMs known for their non-linear behavior because of saturation and cross-saturation effects while SPM also exhibits nonlinear behavior in overloaded condition. [5, 16, 27]. In the performed simulations, the saturation model given in [16], modelled by taking the d- and q-axis currents ( $i_d, i_q$ ) as a function of the d- and q-axis flux linkages ( $\psi_d, \psi_q$ ) is used for the evaluation of the saturation and cross-saturation. The algebraic model for the magnetic saturation is given as

$$i_d(\psi_d, \psi_q) = \psi_d \left( a_{d0} + a_{dd} |\psi_d|^S + \frac{a_{dq}}{V+2} |\psi_d|^U |\psi_q|^{V+2} \right) \quad (4.1a)$$

$$i_q(\psi_d, \psi_q) = \psi_q \left( a_{q0} + a_{qq} |\psi_q|^T + \frac{a_{dq}}{U+2} |\psi_d|^{U+2} |\psi_q|^V \right) \quad (4.1b)$$

where  $S, T, U, V$  are non-negative exponents and  $a_{d0}, a_{dd}, a_{dq}, a_{q0}$  and  $a_{qq}$  are non-negative coefficients. The parameter fitted for the magnetic saturation are given in 4.3. The d-axis flux linkage calculated by taking the magnetic saturation into account is presented Figure 4.2. Whereas, the q-axis flux linkage calculated by taking the magnetic saturation into account is presented Figure 4.3.

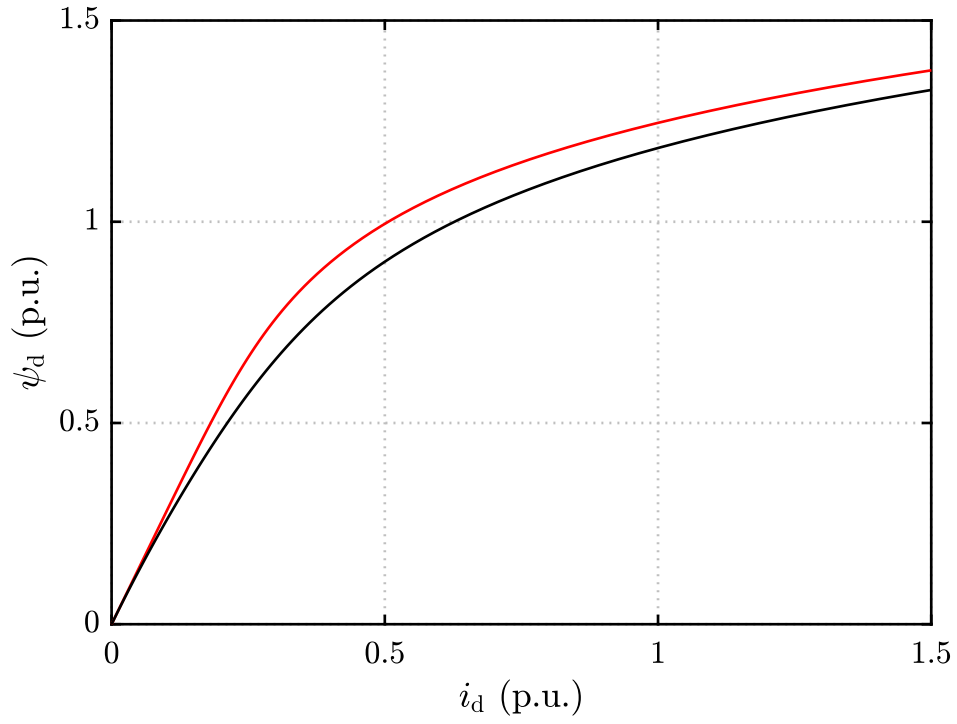


Figure 4.2:  $\psi_d$  as a function of  $i_d$  with  $i_q = [0, 0.6]$  p.u.

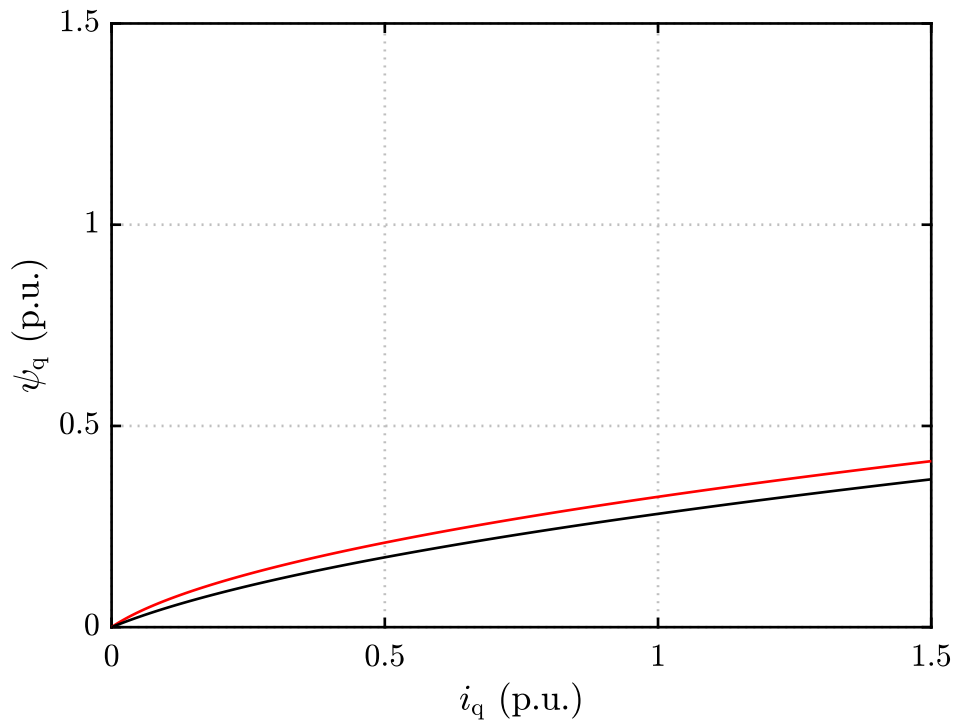


Figure 4.3:  $\psi_q$  as a function of  $i_q$  with  $i_d = [0, 0.3]$  p.u.

Table 4.3: Fitted parameters of SyRM in SI units.

$a_{d0}$	$a_{dd}$	$a_{dq}$	$a_{q0}$	$a_{qq}$	$S$	$T$	$U$	$V$
17.28	369.44	1121.70	52.02	658.59	5	1	1	0

## 4.2 Data Saving Algorithm

An algorithm was written for saving the output voltages ( $u_d, u_q$ ) after the motoring and generating conditions were applied to the motor. Initially, the values from the simulations were loaded and the motor currents and voltages were separated from the other data. The transient states from the current and voltage values were removed and only the data from the steady state was stored. Figure 4.4 illustrates the transient and steady states in the step-wise generation of the d-axis current reference.

After removing the transient state, the even columns of the currents and voltages were flipped so that their average could be taken with the odd columns. After flipping the columns, the average between the even and odd columns of ( $i_d, i_q$ ) and ( $u_d, u_q$ ) was taken and the voltages and currents calculated from the motoring and generating mode were separated. Finally, the d- and q-axis flux linkages were calculated from the average voltage values by using (3.11) and (3.13).

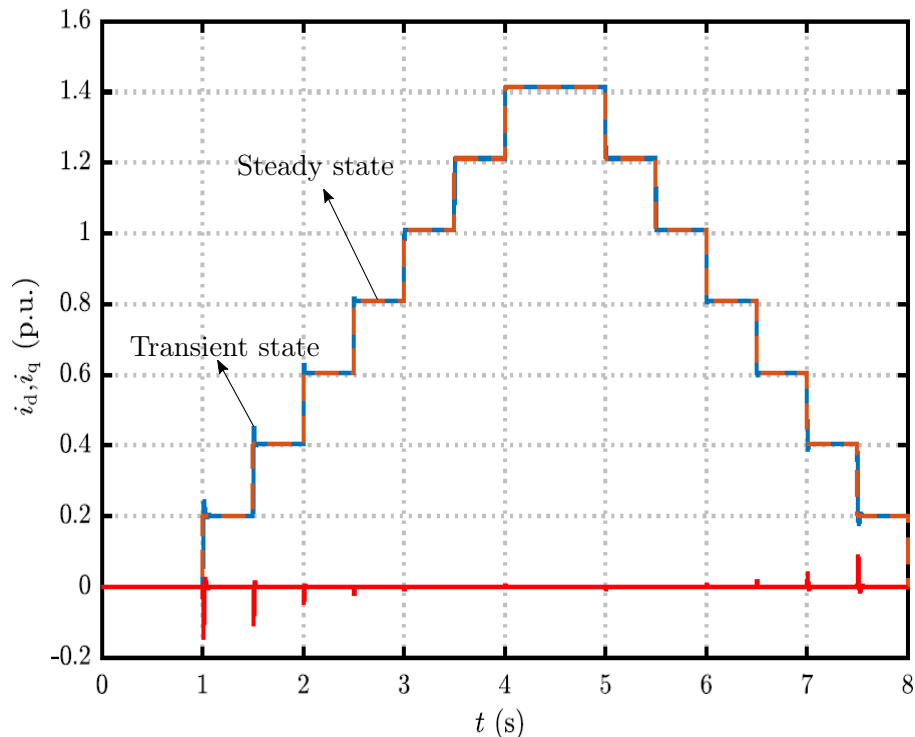


Figure 4.4: Transient and steady states during the d-axis reference current generation.

Table 4.4: Parameters used in simulations for identifying the flux maps.

$f_s$	5 kHz
$\omega_m$	$\frac{\omega_B}{3}$
$N_d$	20
$N_q$	20
$\Delta i_d$	1.55 A
$\Delta i_q$	1.55 A
$t_{id}$	0.5 s
$i_{d,max}$	$\sqrt{2}i_B$
$i_{q,max}$	$\sqrt{2}i_B$

### 4.3 Simulation Results

The parameters used in the reference current generation for identifying the flux maps are given in Table 4.4, where  $i_B$  represents the base value of the current and  $\omega_B$  denotes the base value of the rotor speed. By using these parameters, simulation on a 6.7-kW SyRM were performed. From the simulation results, flux linkages look-up table were produced in terms of the stator currents. The flux maps generated, by using the look-up tables for various current values are divided into following cases.

#### 4.3.1 Case 1

In case 1, the d- and q-axis flux linkages are evaluated for different values of d- and q-axis currents. By using the output voltages corresponding to the motor currents, the flux linkages are calculated in terms of the motor currents using (3.11) and (3.13). For the parameters mentioned in Table 4.4, the flux maps as a function of stator currents are presented in Figure 4.5 and Figure 4.6 respectively. The effect of the cross-saturation can be seen clearly in Figure 4.5 and Figure 4.6 as both the d- and q-axis flux linkages gradually decrease with the increase of the cross current component.

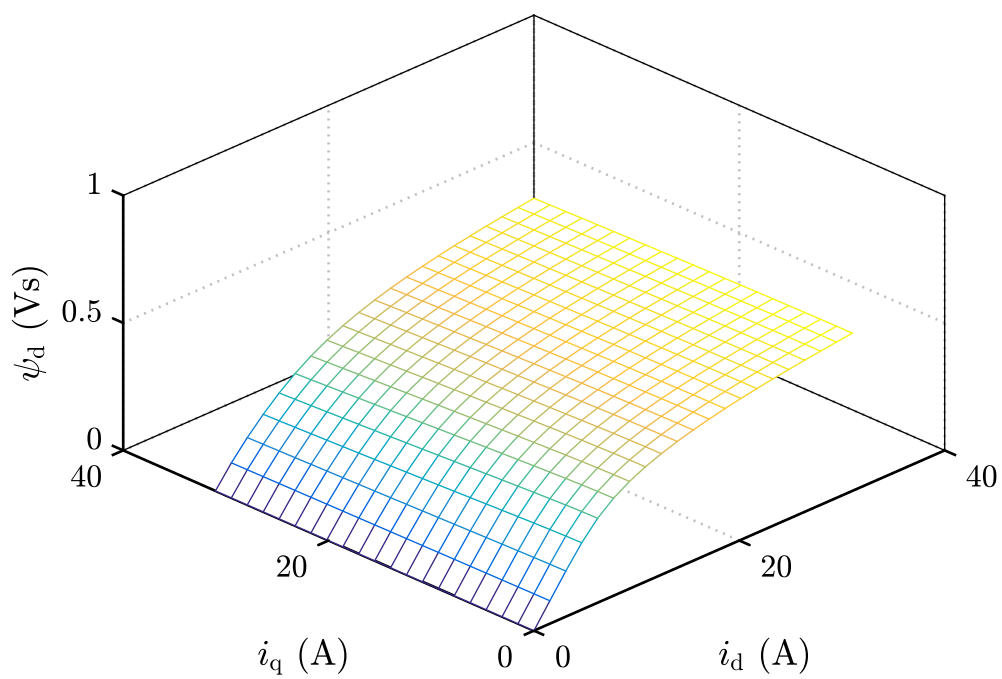
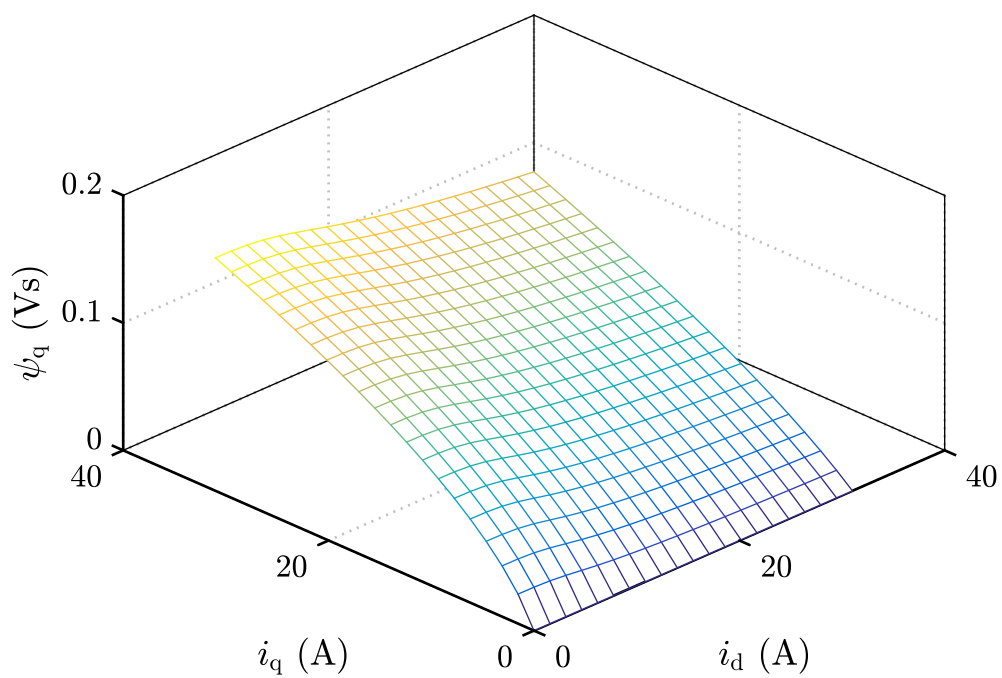
#### 4.3.2 Case 2

In case 2, the d-axis flux linkage was evaluated by taking the self and cross-saturation conditions into account. The d-axis flux linkage calculated with no cross-current component ( $i_q = 0$ ) and the d-axis flux linkage obtained with maximum cross-current component ( $i_q = i_{q,max}$ ) is presented in Figure 4.7. In Figure 4.7, the effect of the cross-saturation in the d-axis flux linkage is clearly visible as with no cross current component, the d-axis flux linkage has a greater value, while with maximum cross current component, the value of  $\psi_d$  is reduced.

### 4.3.3 Case 3

In case 3, the q-axis flux linkage was evaluated by taking the self and cross-saturation conditions into account. The q-axis flux linkage calculated with no cross-current component ( $i_d = 0$ ) and the q-axis flux linkage obtained with maximum cross-current component ( $i_d = i_{d,max}$ ) is presented in Figure 4.8. Similar to  $\psi_d$ , the effect of the cross-saturation in the q-axis flux linkage is visible in Figure 4.8. With no cross current component, the q-axis flux linkage has a higher value, while with maximum cross current component, the value of  $\psi_q$  is decreased.

For all the above mention scenarios, the selection of the correct speed level is of necessary importance. If a low speed value is chosen then the output voltages will contain large number of harmonics that will complicate the process of flux linkage calculation. Conversely, if a high speed value is chosen than significant levels of output voltages will be produced but the iron losses will also increase. When it comes to the selection of the speed value, a trade off between high measurable output voltages and iron losses is required. Normally one third value of the base speed is a good trade off speed.

Figure 4.5:  $\psi_d = \psi_d(i_d, i_q)$ Figure 4.6:  $\psi_q = \psi_q(i_d, i_q)$

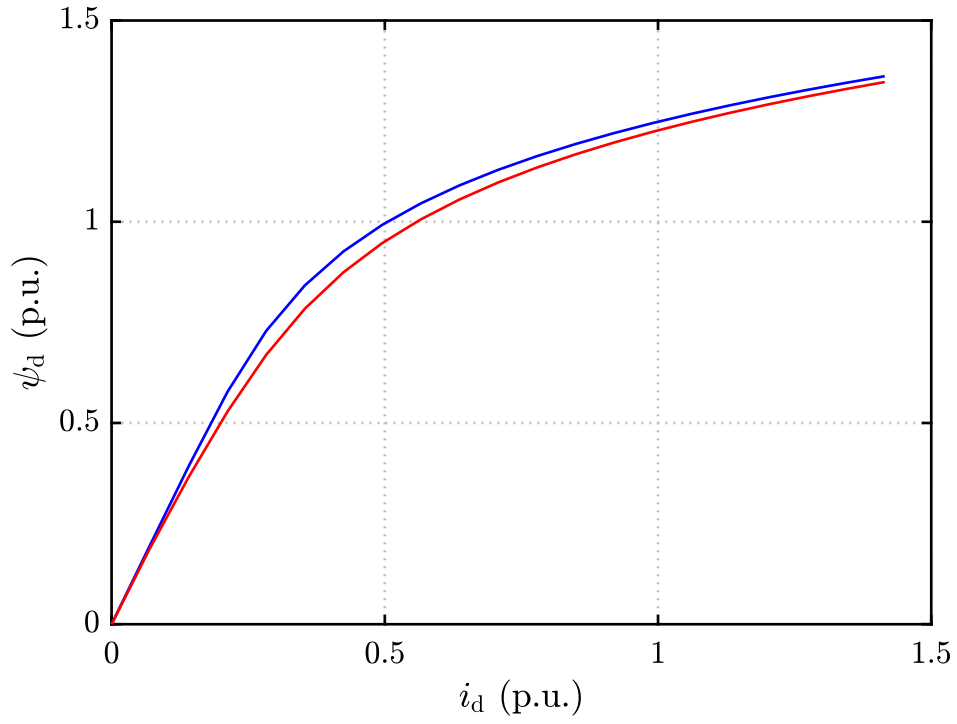


Figure 4.7:  $\psi_d = \psi_d(i_d, 0)$  and  $\psi_d = \psi_d(i_d, i_{q,\max})$

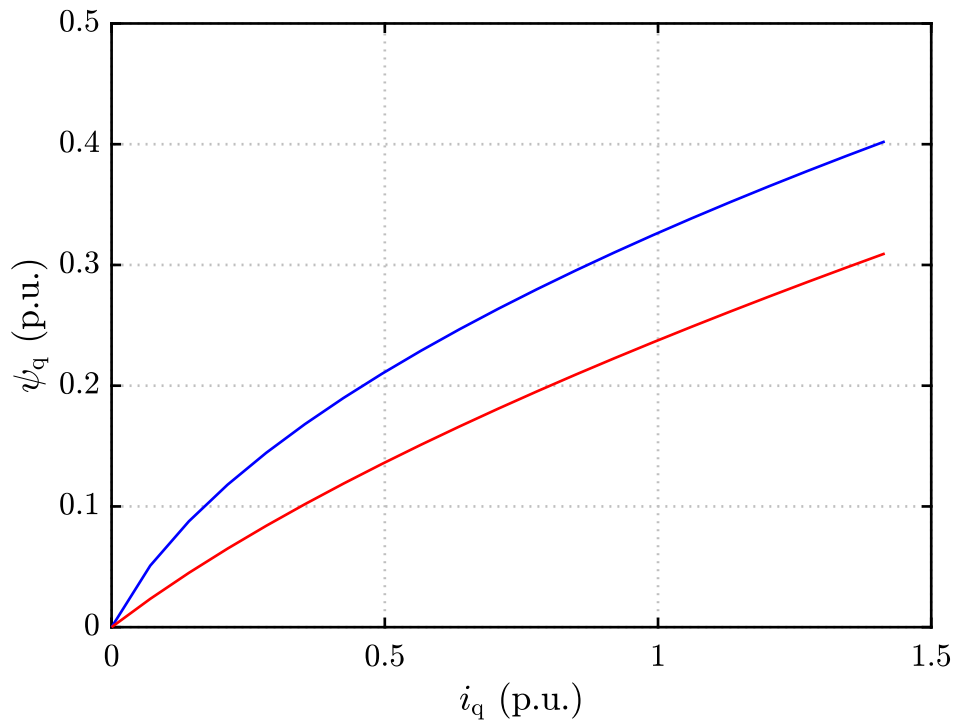


Figure 4.8:  $\psi_q = \psi_q(0, i_q)$  and  $\psi_q = \psi_q(i_{d,\max}, i_q)$

## 5 Conclusions

In this thesis, the flux maps of synchronous machines with a magnetically anisotropic rotor structure such as SyRMs were identified at constant speed. In order to obtain the flux maps, look-up tables of flux linkages in terms of the stator current were calculated. Simulations were performed on a current controlled SyRM for acquiring the flux linkage look-up tables. Operating at constant speed, current sequences were fed to SyRM and the corresponding voltages were calculated. By using the calculated output voltages, the flux linkages were identified as a function of the stator currents and stored in the form of look-up tables.

For the complete and accurate assessment of any kind of motor, the identification of its magnetic model is important. The method presented in this thesis for the evaluation of flux linkages can be used for the magnetic model identification of various kinds of SMs. The flux linkage look-up tables can be used as a benchmark for testing different saturation models of SMs. Besides, being used as a benchmark for testing the saturation models, information about the motor inductances can be obtained through these look-up tables. This information can be used to fully exploit the motor torque and speed range by determining various control strategies such as the maximum torque per ampere and maximum torque per volt.

Various motor manufactures can also benefit from the flux linkage look-up tables obtained in this thesis. For instance, a manufacturer is producing a large number of motors with similar rating, with the help of these flux linkage look-up tables they can identify the characteristics of a single motor in self and cross-saturation conditions and utilize that information for the remaining motors instead of testing each motor separately. These look-up tables also provide useful information for the control purposes of synchronous motors in applications like the sensorless position control at zero or low speed or the deep flux weakening speed range.

The initial objective of this thesis included the experimental identification of flux maps but due to some unforeseen circumstances that was not possible. The process presented in this thesis can be used for the experimental identification of SMs with the help of precise voltage measures exempting the need of some kind of special

hardware. In the future, the algorithm developed in this thesis can be implemented in the laboratory to check the level of accuracy of the estimated flux linkages.

To summarize, the thesis began with the brief introduction of the various types of synchronous motors. Then the modelling of different synchronous motors was discussed which was followed by a brief literature review about the experimental magnetic model identification techniques. After the literature review, the constant speed magnetic model identification method mentioned in [4] was taken as a reference to calculate the flux maps of a SyRM, as a function of motor currents in the rotor synchronous (dq) frame. Finally, the thesis concludes the simulation results obtained from the MATLAB/Simulink environment.

## References

- [1] P. C. Krause, O. Wasynczuk, and S. D. Sudhoff, *Analysis of Electric Machinery and Drive Systems*. Piscataway, NJ: IEEE Press, 2002.
- [2] A. Boglietti and M. Pastorelli, "Induction and synchronous reluctance motors comparison," in *Industrial Electronics, 2008. IECON 2008. 34th Annual Conference of IEEE*, Nov 2008, pp. 2041–2044.
- [3] G. Pellegrino, T. Jahns, N. Bianchi, W. Soong, and F. Cupertino, *The Rediscovery of Synchronous Reluctance and Ferrite Permanent Magnet Motors: Tutorial Course Notes*. Springer International Publishing, 2016.
- [4] E. Armando, R. I. Bojoi, P. Guglielmi, G. Pellegrino, and M. Pastorelli, "Experimental identification of the magnetic model of synchronous machines," *IEEE Transactions on Industry Applications*, vol. 49, no. 5, pp. 2116–2125, Sept 2013.
- [5] B. Stumberger, G. Stumberger, D. Dolinar, A. Hamler, and M. Trlep, "Evaluation of saturation and cross-magnetization effects in interior permanent-magnet synchronous motor," *IEEE Transactions on Industry Applications*, vol. 39, no. 5, pp. 1264–1271, Sept 2003.
- [6] A. Kilthau and J. M. Pacas, "Appropriate models for the control of the synchronous reluctance machine," in *Industry Applications Conference, 2002. 37th IAS Annual Meeting. Conference Record of the*, vol. 4, Oct 2002, pp. 2289–2295 vol.4.
- [7] T. Frenzke, "Impacts of cross-saturation on sensorless control of surface permanent magnet synchronous motors," in *Power Electronics and Applications, 2005 European Conference on*, Sept 2005, pp. 10 pp.–P.10.
- [8] J. D. McFarland, T. M. Jahns, A. M. EL-Refaie, and P. B. Reddy, "Effect of magnet properties on power density and flux-weakening performance of high-speed interior permanent magnet synchronous machines," in *2014 IEEE Energy Conversion Congress and Exposition (ECCE)*, Sept 2014, pp. 4218–4225.
- [9] P. Sekerak, V. Hrabovcova, J. Pyrhonen, L. Kalamen, P. Rafajdus, and M. Onufer, "Comparison of synchronous motors with different permanent magnet and winding types," *IEEE Transactions on Magnetics*, vol. 49, no. 3, pp. 1256–1263, March 2013.
- [10] L. Fang, B. H. Lee, J. J. Lee, H. J. Kim, and J. P. Hong, "Study on high-efficiency characteristics of interior permanent magnet synchronous motor with different magnet material," in *2009 International Conference on Electrical Machines and Systems*, Nov 2009, pp. 1–4.
- [11] K. M. Rahman and S. Hiti, "Identification of machine parameters of a synchronous motor," *IEEE Transactions on Industry Applications*, vol. 41, no. 2, pp. 557–565, March 2005.

- [12] R. Dutta and M. F. Rahman, "A comparative analysis of two test methods of measuring d - and q -axes inductances of interior permanent-magnet machine," *IEEE Transactions on Magnetics*, vol. 42, no. 11, pp. 3712–3718, Nov 2006.
- [13] E. Armando, P. Guglielmi, G. Pellegrino, M. Pastorelli, and A. Vagati, "Accurate modeling and performance analysis of ipm-pmsr motors," *IEEE Transactions on Industry Applications*, vol. 45, no. 1, pp. 123–130, Jan 2009.
- [14] G. Stumberger, T. Marcic, B. Stumberger, and D. Dolinar, "Experimental method for determining magnetically nonlinear characteristics of electric machines with magnetically nonlinear and anisotropic iron core, damping windings, and permanent magnets," *IEEE Transactions on Magnetics*, vol. 44, no. 11, pp. 4341–4344, Nov 2008.
- [15] L. Peretti, P. Sandulescu, and G. Zanuso, "Self-commissioning of flux linkage curves of synchronous reluctance machines in quasi-standstill condition," *IET Electric Power Applications*, vol. 9, no. 9, pp. 642–651, 2015.
- [16] Z. Qu, T. Tuovinen, and M. Hinkkanen, "Inclusion of magnetic saturation in dynamic models of synchronous reluctance motors," in *2012 XXth International Conference on Electrical Machines*, Sept 2012, pp. 994–1000.
- [17] S. Yamamoto, T. Ara, and K. Matsuse, "A method to calculate transient characteristics of synchronous reluctance motors considering iron loss and cross-magnetic saturation," *IEEE Transactions on Industry Applications*, vol. 43, no. 1, pp. 47–56, Jan 2007.
- [18] M. Hinkkanen, P. Pescetto, E. Molsa, S. E. Saarakkala, G. Pellegrino, and R. Bojoi, "Sensorless self-commissioning of synchronous reluctance motors at standstill without rotor locking," *IEEE Transactions on Industry Applications*, vol. PP, no. 99, pp. 1–1, 2016.
- [19] N. Bedetti, S. Calligaro, and R. Petrella, "Stand-still self-identification of flux characteristics for synchronous reluctance machines using novel saturation approximating function and multiple linear regression," *IEEE Transactions on Industry Applications*, vol. 52, no. 4, pp. 3083–3092, July 2016.
- [20] J. Ruan and S. Wang, "A prediction error method-based self-commissioning scheme for parameter identification of induction motors in sensorless drives," *IEEE Transactions on Energy Conversion*, vol. 30, no. 1, pp. 384–393, March 2015.
- [21] G. Pellegrino, R. I. Bojoi, P. Guglielmi, and F. Cupertino, "Accurate inverter error compensation and related self-commissioning scheme in sensorless induction motor drives," *IEEE Transactions on Industry Applications*, vol. 46, no. 5, pp. 1970–1978, Sept 2010.
- [22] G. Pellegrino, B. Boazzo, and T. M. Jahns, "Magnetic model self-identification for pm synchronous machine drives," *IEEE Transactions on Industry Applications*, vol. 51, no. 3, pp. 2246–2254, May 2015.

- [23] J. Holtz and J. Quan, "Sensorless vector control of induction motors at very low speed using a nonlinear inverter model and parameter identification," *IEEE Transactions on Industry Applications*, vol. 38, no. 4, pp. 1087–1095, Jul 2002.
- [24] J. S. Yim, S. K. Sul, B. H. Bae, N. R. Patel, and S. Hiti, "Modified current control schemes for high-performance permanent-magnet ac drives with low sampling to operating frequency ratio," *IEEE Transactions on Industry Applications*, vol. 45, no. 2, pp. 763–771, March 2009.
- [25] J. S. Lee, C. H. Choi, J. K. Seok, and R. D. Lorenz, "Deadbeat-direct torque and flux control of interior permanent magnet synchronous machines with discrete time stator current and stator flux linkage observer," *IEEE Transactions on Industry Applications*, vol. 47, no. 4, pp. 1749–1758, July 2011.
- [26] M. Hinkkanen, H. A. A. Awan, Z. Qu, T. Tuovinen, and F. Briz, "Current control for synchronous motor drives: Direct discrete-time pole-placement design," *IEEE Transactions on Industry Applications*, vol. 52, no. 2, pp. 1530–1541, March 2016.
- [27] P. Guglielmi, M. Pastorelli, and A. Vagati, "Impact of cross-saturation in sensorless control of transverse-laminated synchronous reluctance motors," *IEEE Transactions on Industrial Electronics*, vol. 53, no. 2, pp. 429–439, April 2006.